THE DAMPING OF SECOND SOUND NEAR THE SUPERFLUID TRANSITION IN ^{4}HE

by

BRADLEY J. ROBINSON

B.Sc., University of Toronto, 1972

B.Ed., University of Toronto, 1973

M.Sc., University of British Columbia, 1976

A THESIS SUBMITTED IN PARTIAL FULFILMENT OF

THE REQUIREMENTS FOR THE DEGREE OF

DOCTOR OF PHILOSOPHY

in

THE FACULTY OF GRADUATE STUDIES

(Department of Physics)

We accept this thesis as conforming

to the required standard

THE UNIVERSITY OF BRITISH COLUMBIA

May 1981

In presenting this thesis in partial fulfilment of the requirements for an advanced degree at the University of British Columbia, I agree that the Library shall make it freely available for reference and study. I further agree that permission for extensive copying of this thesis for scholarly purposes may be granted by the Head of my Department or by his representatives. It is understood that copying or publication of this thesis for financial gain shall not be allowed without my written permission.

Department of Physics

The University of British Columbia
2075 Wesbrook Place
Vancouver, Canada
V6T 1W5

Date June 10 1981

ABSTRACT

The attenuation of second sound near the superfluid transition in ^{4}He has been determined by measuring the decay time for free oscillations of plane wave modes in a resonant cavity. The results for both the critical exponent and amplitude of the second sound damping coefficient are consistent with the early predictions of Hohenberg, Siggia and Halperin based on renormalization group theory. However, the damping observed in this work is less than the recent predictions of a non-linear renormalization group analysis by Dohm and Folk.

The measurements cover the temperature interval $1.8 \times 10^{-5} \lesssim t \lesssim 2.1 \times 10^{-2}$, where $t = (T_\lambda - T)/T_\lambda$. Fitting the results to a single power law for $t < 10^{-3}$, the critical exponent governing the temperature dependence is found to be 0.31 ± 0.05. If the results are constrained to obey the theoretical asymptotic temperature dependence with an exponent of 0.288, then the amplitude obtained for the damping is 3.7 ± 0.4 cm^2 s^{-1}. This corresponds to a value for the universal amplitude ratio, R_2, of 0.11 ± 0.01. For $t \gtrsim 10^{-3}$ the damping departs from the critical behaviour, and increases to obtain the values previously observed by Hanson and Pellam for $t \gtrsim 10^{-2}$.

TABLE OF CONTENTS

LIST OF FIGURES

ACKNOWLEDGEMENTS

I am grateful to Dr. M. Crooks for his supervision of this work. I also wish to thank Dr. J. Carolan for his supervision of the final stages of this work while Dr. Crooks was on sabbatical.

Dr. W. Hardy proposed the technique of measuring the decay times. I am indebted to him for this, and several helpful discussions.

CHAPTER 1

INTRODUCTION

This chapter begins with a brief chronological review of the theoretical advances in the field of critical phenomena and an indication of the motivation for this study. In section B the problem addressed in this thesis is described in more detail through a review of other work and a discussion of the implications of recent developments. The theoretical ideas concerning the dynamics of superfluid helium in relation to second sound attenuation are presented in section C.

A. Introduction to Critical Phenomena

A material with a temperature approaching the critical value of a phase transition displays singular behaviour in a variety of both static and dynamic properties. A few examples of critical points are: the Curie point in ferromagnets, the superconducting transition occurring in many metals, the critical point of gas-liquid transitions, the lambda line or superfluid transition in helium.

The initial efforts to describe the form of critical point singularities are reffered to as classical or mean field theories[1]. These were developed around 1900 and include Van der Waals equation for a fluid, the Weiss molecular field theory of ferromagnetism, and the Ornstein-Zernicke equations for correlation functions. These theories are quantitatively incorrect in the critical region, but achieve partial success in that they yield appropriate qualitative behaviour in the form of singularities which can be expressed in terms of critical exponents. Thus, a singularity in the temperature (T) dependence of a physical quantity, A, with critical

exponent, $\bar{a}$, is described by $A = A_o |(T - T_c)/ T_c|^{\bar{a}}$ where T_c is the critical temperature and A_o is the amplitude of the singularity. In 1937 Landau[2] proposed a general theory of the continuous or second order phase transition. His work results in the same exponents as the classical theories and consequently is incorrect. However, he does advance the concept of an order parameter - a central element in modern theories. The generalization to include dynamic properties occurred in 1954 with the introduction of an equation of motion for the order parameter[2]. Equations of this type are employed in current time-dependent Ginzburg-Landau models.

In the mid-sixties there evolved a phenomenological treatment of phase transitions known as scaling[3]. This theory predicts relationships or scaling laws which exist among various critical exponents and therefore escapes the limits of mean field theory. By the end of the sixties the extension of scaling to include dynamic properties had been accomplished[4]. Along with scaling there developed a related concept known as universality. Initially formulated as the law of corresponding states, the hypothesis of universality means that relatively few fundamentally different types or classes of critical behaviour are sufficient to accommodate a complete categorization of phase transtions. In particular, the entire lambda line in liquid helium is in one universality class and therefore the effects of elevated pressure should be mild in the sense that, for example, exponents remain unchanged.

During the last decade the renormalization group methods of quantum field theory have been applied, with great success, to the problem of both static[5] and dynamic[6] critical phenomena. Renormalization group theory (RGT) provides a more fundamental derivation of scaling, as well as a means of calculating critical exponents and the values of certain amplitude ratios. On the basis of RGT there is a concrete formulation of univer-

sality in which the equivalence classes are essentially determined by the dimensionality, d, of the system and the number of components, n, in the order parameter. The transformations involved in this theory are sufficiently complex that results can usually be evaluated only approximately with expansions in 4-d or 1/n. Indeed, the mathematical structure of the RG as well as its application to physical systems is the subject of much current research.

The initial motivation for this work was based on one of the predictions of dynamic scaling related to the damping of second sound near the lambda transition in liquid helium. Second sound is a propagating mode of thermal transport which appears as a temperature-entropy wave in the low temperature superfluid phase of ^{4}He. It was felt that precise measurements of the critical damping at various pressures would provide a severe test of both scaling and universality. This prediction, the experimental situation regarding second sound damping, and the implications for this work which resulted from the advent of RGT are the subject of the following section.

B. Review of Second Sound Damping

The earliest measurements of the attenuation, α_2, of second sound relevant to this work are those of Hanson and Pellam (HP) in 1954[7]. From their data it is possible to extract the, now more pertinent, damping coefficient D_2 by means of the hydrodynamic expression

$$\alpha_2(\omega,T) = \tfrac{1}{2}(\omega^2/u_2^3)\, D_2(T) \qquad (1)$$

where ω is the angular frequency of the second sound with velocity u_2. This expression is derived in section C and, as indicated by the notation, in the regime of hydrodynamics D_2 depends only on temperature. The range of temperatures covered by HP are such that $\Delta T = T_\lambda - T \gtrsim 10^{-2}$ K and there-

fore do not enter deeply into the critical region. However, their measurements are important in the interpretation of the results of this work and will be discussed in later chapters.

As previously mentioned, theoretical work in the late sixties resulted in the dynamic scaling prediction of the critical temperature dependence of D_2:

$$D_2 \propto u_2 \xi \tag{2}$$

where ξ is the correlation length for fluctuations of the order parameter. The arguments used to arrive at this result are outlined in section C. In view of the proportionality, the experimental verification of relation (2) will involve only the exponents which govern the behaviour of each quantity as $T \to T_\lambda$. From the two-fluid hydrodynamic expression for u_2 (see Eq. (26) in section C), the terms with a significant dependence on ΔT indicate $u_2 \propto (\rho_s/c_p)^{\frac{1}{2}}$ where ρ_s is the density of the superfluid component and c_p is the specific heat at constant pressure. The definition of a correlation length for a power law decay of the correlation function at large distances, as is the case for helium with $T < T_\lambda$, and the formulation of hydrodynamics in terms of correlation functions yields $\xi \propto \rho_s^{-1}$. Therefore, the scaling prediction (2) becomes $D_2 \propto (c_p \rho_s)^{-\frac{1}{2}}$. The exponent for $\rho_s \propto (\Delta T)^\zeta$ has been found to be $\zeta = 0.666 \pm 0.006$ from an Andronikashvili-type experiment[8]. Alternatively, ρ_s may be derived from measurements of u_2 (plus other empirical information and the hydrodynamic expression for u_2) with the result $\zeta = 0.674 \pm 0.001$ at saturated vapour pressure[9]. The specific heat, c_p, increases slowly with a near logarithmic dependence on ΔT as ΔT decreases. Thus measurements of D_2 would verify dynamic scaling to the extent that they confirm

$$D_2 \propto (c_p)^{-\frac{1}{2}} (\Delta T)^{-\zeta/2} \sim (\Delta T)^{-1/3} \tag{3}.$$

Prior to the beginning of this study an experiment by Tyson[10] provided the only test of relation (3) for the case of macroscopic second sound[11]. His results give 0.34 ± 0.06 for the exponent of D_2 and consequently agree with the value 1/3. However, the results do not confirm the predicted contribution from c_p in (3). This might be expected to lower, to perhaps 0.28, the exponent which would be calculated from a power law fit to the data for $D_2(\Delta T)$ over the temperature range of his experiment. Initially one of the objectives of this work was to obtain more precise values of D_2 in order to establish or deny the presence of c_p and so provide a stringent test of the details of dynamic scaling. The second objective was to test the universality of the scaling relation (2) by performing the measurements of critical damping under pressure. There was, and still is, no such information on D_2 available.

The renormalization group treatment of a dynamic model[6] of helium confirms the scaling relation (2), and provides a means of calculating the universal constant defined by the ratio $R_2 = D_2/2u_2\xi$. The theoretically estimated value for R_2, given in the next section, has been found to be a factor of about five smaller than that indicated by Tyson's data. This discrepancy had serious implications in the initial stages of this work. If the smaller value of R_2 as predicted by theory was in fact correct, then a considerable improvement in the experimental error, compared to that obtained by Tyson, would be required in order to resolve the predicted temperature dependence of D_2.

During the course of this work, Tanaka and Ikushima[12] have interpreted their studies on thermal transport in ^3He - ^4He mixtures as evidence in support of the value of R_2 obtained from Tyson's data. Recently Ahlers[13] has reported results on second sound damping which are in agreement with

the value of R_2 initially calculated by Hohenberg, Siggia and Halperin (HSH)[14] on the basis of RGT. More recently, a nonlinear renormalization group analysis of the dynamics of the superfluid transition by Dohm and Folk (DF)[15] has resulted in predictions concerning second sound damping which are also in agreement with the work of Ahlers; however, their theory predicts a temperature dependence for the effective ratio $R_2^{eff}(\Delta T/T_\lambda)$ which enters the equation, $D_2 = R_2^{eff} 2u_2\xi$, governing the behaviour of D_2. Also, their predictions for D_2 cover a larger temperature interval extending beyond the critical region.

In view of the theoretical and experimental status of D_2 outlined above, the results of this work are significant in that they confirm the results of Ahlers. In addition, since the measurements of this work are of greater accuracy and cover a larger temperature interval, they provide a more severe test of the theoretical predictions of HSH and DF, and indicate the behaviour of D_2 in the temperature interval between the previously existing experimental data in the critical and non-critical regions.

C. The Dynamics of Superfluid Helium

i) Hydrodynamics and the Damping Coefficient D_2

The hydrodynamics of the two fluid model of superfluid helium is reviewed here. This theory is relevant to an understanding of second sound and the mechanisms responsible for its damping, as well as providing the foundation and interpretation of the dynamic models employed in scaling and RGT.

The two fluid model obtains some microscopic justification in the quasi-particle (elementary excitation) theory of Landau[16], and more recently in the theory of Hohenberg and Martin[17] based on the assumption of a Bose condensate. This model describes He II in terms of interpenetrating

normal and superfluid components with densities ρ_n and ρ_s respectively. The velocity fields associated with these components are $\vec{v}_n$ and $\vec{v}_s$, subject to the irrotational condition on $\vec{v}_s$

$$\text{curl } \vec{v}_s = 0, \tag{4}$$

provided $\vec{v}_n$ and $\vec{v}_s$ are below some critical value. In the approximation in which dissipative effects are neglected, a typical derivation[16,18] of the hydrodynamic equations begins with the conservation laws and an equation of motion for $\vec{v}_s$ satisfying (4). Thus

$$\frac{\partial \rho}{\partial t} + \text{div } \vec{j} = 0 \tag{5-A}$$

expresses mass conservation in terms of liquid density ρ and mass current $\vec{j} = \{j_i\}$ which is the momentum per unit volume;

$$\frac{\partial j_i}{\partial t} + \frac{\partial \Pi_{ik}}{\partial x_k} = 0 \quad \text{(summation convention)} \tag{5-B}$$

is the statement of momentum conservation where Π_{ik} is the momentum flux density tensor; the absence of dissipation is written as conservation of entropy

$$\frac{\partial \rho\sigma}{\partial t} + \text{div } \vec{F} = 0 \tag{5-C}$$

where σ is the entropy per unit mass and $\vec{F}$ is the entropy flux; the irrotational character of the superfluid velocity field means that the time development of $\vec{v}_s$ satisfies an equation of the form

$$\frac{\partial \vec{v}_s}{\partial t} + \text{grad } (\tfrac{1}{2}v_s^2 + h) = 0 \tag{5-D}$$

where h is a scalar function. These, (5-A,B,C,D), are eight equations for the eight basic variables ρ, σ, $\vec{v}_s$, $\vec{j}$ in terms of the yet to be determined quantities Π_{ik}, $\vec{F}$, h. Conservation of energy,

$$\frac{\partial U}{\partial t} + \text{div } \vec{Q} = 0 \tag{6}$$

where U is the energy per unit volume and $\vec{Q}$ is the energy flux density, is a ninth and hence redundant equation which must be automatically satisfied by (5-A,B,C,D). This constraint, the application of Galilean relativity and thermodynamic arguments are sufficient to determine Π_{ik}, $\vec{F}$, h under the assumption that they do not contain dissipative contributions in the form of spatial gradients of thermodynamic variables.

In the determination of Π_{ik}, $\vec{F}$, h the existence of two independent velocity fields is significant to the thermodynamics since it is not generally possible to transform to a frame in which the fluid is at rest. Thus, there appears an additional conjugate pair of thermodynamic variables arising from the relative internal velocity. Consider a Galilean transformation relating two frames denoted by subscripts 1 and 2 and with relative velocity $\vec{v}_r$. The relations for velocity, momentum and energy density are $\vec{v}_2 = \vec{v}_1 + \vec{v}_r$, $\vec{j}_2 = \vec{j}_1 + \rho\vec{v}_r$, $U_2 = U_1 + \vec{v}_r \cdot \vec{j}_1 + \frac{1}{2}\rho v_r^2$. An energy density which satisfies this transformation is

$$U = U_o + \vec{v}_s \cdot (\vec{j} - \rho\vec{v}_s) + \tfrac{1}{2}\rho v_s^2 \tag{7}$$

where U_o is a Galilean invariant and represents the energy density in a frame in which the superfluid is at rest. As U_o is an invariant its dependence on the basic variables ρ, σ, $\vec{j}$, $\vec{v}_s$ is

$$dU_o = \mu d\rho + T d(\rho\sigma) + \vec{w} \cdot d(\vec{j} - \rho\vec{v}_s) \tag{8}$$

since $\vec{j} - \rho\vec{v}_s$ is invariant. In (8) $\vec{w}$ is the conjugate to $\vec{j} - \rho\vec{v}_s$ (as μ is to ρ and T is to $\rho\sigma$) and serves to define $\vec{v}_n$ via $\vec{w} = \vec{v}_n - \vec{v}_s$. Then, the last term in (8) states that the derivative of energy with respect to momentum is velocity. With expressions (7) and (8) for the energy density, the constraint imposed by energy conservation can be used to determine Π_{ik}, $\vec{F}$, h. By differentiating U with respect to time and then replacing all time derivatives by spatial derivatives through the use of equations

(5-A,B,C,D), it is possible to identify the energy flux density $\vec{Q}$ as well as Π_{ik}, $\vec{F}$, h. The algebra can be found in considerable detail in reference 18. The results become intuitively appealing when the basic variable set is taken to be ρ, σ, $\vec{v}_n$, $\vec{v}_s$ where $\vec{v}_n$ is related to $\vec{j}$ by

$$\vec{j} = \rho_n \vec{v}_n + \rho_s \vec{v}_s \text{ with } \rho_n + \rho_s = \rho \tag{9}.$$

Then the expression for Π_{ik} is

$$\Pi_{ik} = p\delta_{ik} + \rho_s v_{si} v_{sk} + \rho_n v_{ni} v_{nk} \tag{10}$$

where p is the pressure. Thus, Π_{ik} appears as a natural generalization of the momentum flux density $P_{ik} = p\delta_{ik} + \rho v_i v_k$ in single fluid hydrodynamics. The result for the entropy flux vector is

$$\vec{F} = \rho\sigma\vec{v}_n \tag{11}$$

which means that all entropy is carried by the normal fluid. The scalar function

$$h = \mu \tag{12}$$

is the chemical potential. The quantities μ, p, ρ_n which now appear are functions of ρ, σ as well as $(\vec{v}_n - \vec{v}_s)^2$. Thus, the hydrodynamic equations, neglecting dissipation are (5-A,B,C,D) with $\vec{j}$, Π_{ik}, $\vec{F}$, h given by (9, 10, 11, 12). Before discussing wave solutions to these equations, they will be augmented to include dissipation in anticipation of obtaining a hydrodynamic expression for second sound attenuation.

Dissipation is a consequence of the irreversible processes associated with thermal conduction and the viscosity or internal friction which results from internal motion. These irreversible processes occur when there are departures from equilibrium and cause the system to move towards an equilibrium state characterized by a maximum in the entropy. Thus, the approach to equilibrium involves entropy production, Σ/T, and the generalization to equation (5-C) is

$$\frac{\partial \rho\sigma}{\partial t} + \text{div}\ (\rho\sigma\vec{v}_n + \frac{\vec{q}}{T}) = \frac{\Sigma}{T} \qquad (13\text{-C}).$$

The dissipative contribution to entropy flux, $\vec{q}/T$, is, of course, identified in lowest order with thermal conduction. Admitting a dissipative contribution, h', to the superfluid flow but still requiring curl $\vec{v}_s = 0$, the superfluid acceleration equation (5-D) becomes

$$\frac{\partial \vec{v}_s}{\partial t} + \text{grad}\ (\mu + \tfrac{1}{2}v_s^2 + h') = 0 \qquad (13\text{-D}).$$

There still remain the conservation laws for mass, momentum and energy. The equation for mass conservation or continuity is unchanged:

$$\frac{\partial \rho}{\partial t} + \text{div}\ \vec{j} = 0 \qquad (13\text{-A}).$$

With a viscous stress tensor τ_{ik} the momentum equation is

$$\frac{\partial j_i}{\partial t} + \frac{\partial (\Pi_{ik} + \tau_{ik})}{\partial x_k} = 0 \qquad (13\text{-B}).$$

Energy conservation is now

$$\frac{\partial U}{\partial t} + \text{div}\ (\vec{Q} + \vec{Q}') = 0 \qquad (14)$$

where $\vec{Q}'$ is the additional dissipative energy flux density.

The form of Σ, $\vec{q}$, h', τ_{ik} must now be determined. As in the non-dissipative case the energy equation (14) must be satisfied automatically. By differentiating with respect to time the expression for the internal energy (7, 8) and replacing time derivatives by spatial ones through the use of (13-A,B,C,D), a pure divergence term may be identified with $\vec{Q} + \vec{Q}'$, while the remainder must vanish. This yields for the entropy production

$$\Sigma = -\frac{\vec{q}\cdot\vec{\nabla}T}{T} - \tau_{ik}\frac{\partial v_{ni}}{\partial x_k} - h'\vec{\nabla}\cdot\rho_s(\vec{v}_s - \vec{v}_n) \qquad (15).$$

The entropy production must be positive definite and vanish in equilibrium. This requirement, and those based on Galilean covariance, are sufficient

to determine expressions for the fluxes $\vec{q}$, τ_{ik}, h' which, to first order in the deviations (spatial derivatives) from equilibrium, involve thirteen independent kinetic coefficients. At this level $\vec{v}_n - \vec{v}_s$ is not considered small since in the equilibrium state of solid body rotation $\vec{v}_n - \vec{v}_s$ can be large due to the presence of superfluid vortices. However, in the limit of small deviations from a non-rotating equilibrium state, as applies to this work, $\vec{v}_n - \vec{v}_s$ is also small. Then there appear kinetic coefficients in the fluxes as follows:

$$\vec{q} = -\kappa\vec{\nabla} T \tag{16}$$

where κ is the coefficient of thermal conduction,

$$\tau_{ij} = -\eta\left(\frac{\partial v_{ni}}{\partial x_j} + \frac{\partial v_{nj}}{\partial x_i} - \frac{2}{3}\delta_{ij}\vec{\nabla}\cdot\vec{v}_n\right) - \delta_{ij}\left(\zeta_1\vec{\nabla}\cdot\rho_s(\vec{v}_s-\vec{v}_n) + \zeta_2\vec{\nabla}\cdot\vec{v}_n\right) \tag{17}$$

and

$$h' = -\zeta_3\vec{\nabla}\cdot\rho_s(\vec{v}_s - \vec{v}_n) - \zeta_4\vec{\nabla}\cdot\vec{v}_n \tag{18}.$$

In the viscous stress tensor, τ_{ij}, there are the usual coefficients of first and second viscosity, η and ζ_2, which appear in the "normal" fluid hydrodynamics. Due to the additional degree of freedom allowed by $\vec{v}_s$, there appears in τ_{ij} another second viscosity, ζ_1, which determines the dissipation generated by relative motion, $\vec{v}_n - \vec{v}_s$. The dissipative correction, h', to the chemical potential contains two more coefficients of second viscosity ζ_3, ζ_4; however, by the Onsager reciprocity theorem, $\zeta_4 = \zeta_1$, so that there are five independent kinetic coefficients. Also, $\Sigma > 0$ requires that κ, η, ζ_2, ζ_3 be positive and $\zeta_1^2 < \zeta_2\zeta_3$.

The characteristics of sound propagation can now be analyzed on the basis of the hydrodynamic equations, (13-A,B,C,D), with the substitutions (15, 16, 17, 18). The equations for ρ, σ, $\vec{v}_s$, $\vec{v}_n$ are written in linearized form by means of

$$\rho = \rho_o + \delta\rho \qquad \sigma = \sigma_o + \delta\sigma$$

$$p = p_o + \delta p \qquad T = T_o + \delta T$$

$$\vec{v}_n = \delta\vec{v}_n \qquad \vec{v}_s = \delta\vec{v}_s \quad .$$

The disturbances, δ, contain the space and time dependence. The equilibrium state, denoted by a subscript 'o', is one in which $\vec{v}_n - \vec{v}_s = 0$. The linearized, that is, to order δ, equations including dissipation are then

$$\frac{\partial\delta\rho}{\partial t} + \rho_{no}\frac{\partial\delta v_{ni}}{\partial x_i} + \rho_{so}\frac{\partial\delta v_{si}}{\partial x_i} = 0 \qquad (19\text{-A}),$$

$$\rho_{no}\frac{\partial\delta v_{ni}}{\partial t} + \rho_{so}\frac{\partial\delta v_{si}}{\partial t} + \frac{\partial\delta p}{\partial x_i} = \eta\frac{\partial}{\partial x_j}\left(\frac{\partial\delta v_{ni}}{\partial x_j} + \frac{\partial\delta v_{nj}}{\partial x_i} - \frac{2}{3}\delta_{ij}\frac{\partial\delta v_{n\ell}}{\partial x_\ell}\right)$$

$$+ \frac{\partial}{\partial x_i}\left(\zeta_1\frac{\partial\rho_{so}(\delta v_{sk} - \delta v_{nk})}{\partial x_k} + \zeta_2\frac{\partial v_{nk}}{\partial x_k}\right) \qquad (19\text{-B}),$$

$$\frac{\partial\delta(\rho\sigma)}{\partial t} + \rho_o\sigma_o\frac{\partial\delta v_{nk}}{\partial x_k} = \frac{\kappa}{T}\frac{\partial}{\partial x_i}\cdot\frac{\partial\delta T}{\partial x_i} \qquad (19\text{-C}),$$

and $$\frac{\partial\delta v_{si}}{\partial t} + \frac{\partial\delta\mu}{\partial x_i} = \frac{\partial}{\partial x_i}\left(\zeta_3\frac{\partial\rho_{so}(\delta v_{sk} - \delta v_{nk})}{\partial x_k} + \zeta_4\frac{\partial\delta v_{nk}}{\partial x_k}\right) \qquad (19\text{-D}).$$

In this approximation $\delta\mu$ is just the usual $\delta\mu = (1/\rho)\delta p - \sigma\delta T$. Wave solutions are attempted in the form

$$\delta\rho = \tilde{\rho}e^{-i(\omega t - kx)} = \tilde{\rho}e^{-i\omega(t - x/u)} \quad ,$$

and similarly for $\delta\sigma$, δp, δT, $\delta\vec{v}_n = \delta v_n\hat{x}$, $\delta\vec{v}_s = \delta v_s\hat{x}$. The linearized equations now become, dropping the subscript 'o',

$$-i\omega\tilde{\rho} + ik\rho_n\vec{v}_n + ik\rho_s\vec{v}_s = 0 \qquad (20\text{-A}),$$

$$-i\omega\rho_n\tilde{v}_n - i\omega\rho_s\tilde{v}_s + ik\tilde{p} = -k^2\left(\frac{4}{3}\eta - \rho_s\zeta_1 + \zeta_2\right)\tilde{v}_n - k^2\zeta_1\rho_s\tilde{v}_s \qquad (20\text{-B}),$$

$$-i\omega(\rho\tilde{\sigma} + \tilde{\rho}\sigma) + ik\rho\sigma\tilde{v}_n = -k^2\frac{\kappa}{T}\tilde{T} \qquad (20\text{-C}),$$

$$-i\omega\tilde{v}_s + ik\left(\frac{\tilde{P}}{\rho} - \sigma\tilde{T}\right) = k^2(\zeta_4 - \rho_s\zeta_3)\tilde{v}_n - k^2\zeta_3\rho_s\tilde{v}_s \qquad (20\text{-D}).$$

Thus, there are now four equations for four unknowns $\tilde{\rho}$, $\tilde{\sigma}$, $\tilde{v}_n$, $\tilde{v}_s$. The small variations $\tilde{p}$, $\tilde{T}$ depend in this approximation on $\tilde{\rho}$, $\tilde{\sigma}$ as

$$\tilde{p} = \left(\frac{\partial p}{\partial \rho}\right)_\sigma \tilde{\rho} + \left(\frac{\partial p}{\partial \sigma}\right)_\rho \tilde{\sigma}$$

$$\tilde{T} = \left(\frac{\partial T}{\partial \rho}\right)_\sigma \tilde{\rho} \quad \left(\frac{\partial T}{\partial \sigma}\right)_\rho \tilde{\sigma} \quad .$$

A dispersion relation, $\omega(k)$, can be obtained by eliminating $\tilde{v}_n$, $\tilde{v}_s$ in favour of $\tilde{\rho}$, $\tilde{\sigma}$ and retaining only first order terms in the kinetic coefficients. Equation (20-B) through the use of (20-A) and (20-C) becomes

$$\left(\frac{\omega^2}{k^2} - \frac{\partial p}{\partial \rho}\right)\tilde{\rho} = -i\omega\left\{\frac{1}{\rho}\left(\frac{4}{3}\eta + \zeta_2\right)\tilde{\rho} + \frac{1}{\sigma}\left(\frac{4}{3}\eta - \rho\zeta_1 + \zeta_2\right)\tilde{\sigma}\right\} + \frac{\partial p}{\partial \sigma}\tilde{\sigma} \qquad (21).$$

A second equation is obtained from (20-D) by using (20-B) as an expression for $\tilde{p}$ and subsequently eliminating $\tilde{v}_n$ and $\tilde{v}_s$ by means of (20-A) and (20-C). The result is

$$\left(\sigma\frac{\partial T}{\partial \sigma} - \frac{\omega^2}{k^2}\frac{\rho_n}{\sigma\rho_s}\right)\tilde{\sigma} = +i\omega\left\{\frac{1}{\rho}\left(-\zeta_4 + \frac{\zeta_2}{\rho} + \frac{4}{3}\frac{\eta}{\rho} + \frac{\rho_n}{\rho_s}\frac{\kappa}{\sigma T}\frac{\partial T}{\partial \rho}\right)\tilde{\rho}\right.$$

$$\left. + \frac{1}{\sigma}\left(-\zeta_4 + \rho\zeta_3 + \frac{\zeta_2}{\rho} - \zeta_1 + \frac{4\eta}{3\rho} + \frac{\rho_n}{\rho_s}\frac{\kappa}{\rho T}\frac{\partial T}{\partial \sigma}\right)\tilde{\sigma}\right\}$$

$$- \sigma\frac{\partial T}{\partial \rho}\tilde{\rho} \qquad (22).$$

Consider for the moment the approximation in which dissipation is neglected by ignoring the kinetic coefficients in equations (21) and (22). Then they read

$$\left(\frac{\omega^2}{k^2 u_1^2} - 1\right)\tilde{\rho} - \left(\frac{\partial \rho}{\partial p}\right)_\sigma \left(\frac{\partial p}{\partial \sigma}\right)_\rho \tilde{\sigma} = 0 \qquad (23)$$

$$\left(\frac{\partial T}{\partial \rho}\right)_\sigma \left(\frac{\partial \sigma}{\partial T}\right)_\rho \tilde{\rho} + \left(1 - \frac{\omega^2}{k^2 u_2^2}\right)\tilde{\sigma} = 0 \qquad (24)$$

with $u_1^2 = (\partial p/\partial \rho)_\sigma$ and $u_2^2 = (\rho_s/\rho_n)\sigma^2(\partial T/\partial \sigma)_\rho = (\rho_s/\rho_n)\sigma^2 T/c_v$. The condition for the compatibility of (23) and (24) is that the determinant of the coefficients vanish. Thus

$$\left(\frac{\omega^2}{k^2 u_1^2} - 1\right)\left(\frac{\omega^2}{k^2 u_2^2} - 1\right) = \left(\frac{\partial \rho}{\partial p}\right)_\sigma \left(\frac{\partial p}{\partial \sigma}\right)_\rho \left(\frac{\partial T}{\partial \rho}\right)_\sigma \left(\frac{\partial \sigma}{\partial T}\right)_\rho$$

$$= (c_p - c_v)/\, c_p \quad .$$

At the saturated vapour pressure and for the values of ΔT in this experiment[19] $(c_p - c_v)/\, c_p \ll 1$, so the approximation that this term is zero results in decoupled modes

$$\frac{\omega}{k} = u_1 = \left(\frac{\partial p}{\partial \rho}\right)_\sigma^{\frac{1}{2}} \tag{25}$$

$$\frac{\omega}{k} = u_2 = \left(\frac{\rho_s}{\rho_n}\ \frac{\sigma^2 T}{c}\right)^{\frac{1}{2}} \quad , \quad c \equiv c_p \simeq c_v \tag{26}$$

known as first and second sound. The first is the usual adiabatic density-pressure sound wave, while second sound is an entropy-temperature wave at constant density.

Now consider the dissipative equations (21) and (22) in the decoupled approximation $(c_p - c_v)/c_p = 0$. To first order in the kinetic coefficients the requirement that the determinant of the coefficients of ρ' and σ' vanish yields dispersion relations as follows:

$$\frac{\omega^2}{k^2} = u_1^2 - i\,\frac{\omega}{\rho}\left(\frac{4}{3}\eta + \zeta_2\right)$$

and $$\frac{\omega^2}{k^2} = u_2^2 - \frac{i\omega}{\rho}\,\frac{\rho_s}{\rho_n}\left(\frac{4}{3}\eta + \rho^2\zeta_3 - \rho(\zeta_1 + \zeta_4) + \zeta_2 + \frac{\rho_n}{\rho_s}\,\frac{\kappa}{c}\right) \tag{27}.$$

Considering the second sound solution, the attenuation can be determined by writing $k = k_o + i\alpha_2$ and expanding to first order. This gives

$$\alpha_2(\omega, T) = \frac{1}{2}\,\frac{\omega^2}{\rho u_2^3}\,\frac{\rho_s}{\rho_n}\left(\frac{4}{3}\eta + \rho^2\zeta_3 - \rho(\zeta_1 + \zeta_4) + \zeta_2 + \frac{\rho_n}{\rho_s}\,\frac{\kappa}{c}\right) .$$

The damping constant D_2 is defined by

$$\alpha_2(\omega,T) = \tfrac{1}{2}(\omega^2/\, u_2^3)\, D_2 \qquad (28).$$

Therefore in linearized hydrodynamics D_2 is independent of frequency and

$$D_2(T) = \frac{\rho_s}{\rho\rho_n}\left(\frac{4}{3}\eta + \rho^2\zeta_3 - \rho(\zeta_1 + \zeta_4) + \zeta_2 + \frac{\rho_n}{\rho_s}\,\frac{\kappa}{c}\right) \qquad (29).$$

Thus, on the basis of hydrodynamics alone, measurements of second sound damping may only be interpreted in terms of a rather lengthy combination of thermodynamic properties. However, some information concerning D_2 can be gained from independent measurement and theoretical calculation of the individual quantities contributing to D_2. In particular, the behaviour of D_2 as $T \to T_\lambda$ is expected to be approximately proportional to $(\Delta T)^{-1/3}$. The contributions to this divergence are as follows. It is known from experiment that $\rho_s \propto (\Delta T)^{2/3}$. The viscosity, η, is measured to be finite at T_λ so its effect on D_2, $\sim \rho_s\eta$, vanishes. The second viscosities ζ_1, ζ_2, ζ_3 are expected, from first sound attenuation measurements and the Landau theory, to vary roughly as $(\Delta T)^{-1}$ and therefore contribute $(\Delta T)^{-1/3}$. The strength of the thermal conductivity term is conjectured. If its behaviour below T_λ (which cannot be measured due to superfluidity) is the same as above, then it is about $(\Delta T)^{-1/3}$. If, as experiments on ^{3}He - ^{4}He mixtures suggest, κ is finite at T_λ, then the growth of the specific heat, c, as $T \to T_\lambda$ would cause $\kappa/\rho c$ to diminish.

The scaling treatment of critical dynamics as it relates to D_2 is now discussed.

ii) Scaling and D_2

Scaling[4] begins with the recognition of the importance of the variable which has the largest fluctuations near the transition and consequently is most responsible for the critical behaviour. This variable, the order par-

amter ψ, has a range, ξ, of correlations in the fluctuations which is divergent as $\xi = \xi_o(\Delta T/T_c)^{-\nu}$. The description of fluctuations of any (Hermitian) variable A(r,t) is done in terms of the correlation function $\tilde{c}^A(r,t)$ defined as

$$\tilde{c}^A(r,t) = \tfrac{1}{2} \left\langle \{ \left(A(r,t) - \langle A(r,t)\rangle\right), \left(A(0,0) - \langle A(0,0)\rangle\right) \} \right\rangle \qquad (30)$$

where the angular bracket denotes equilibrium average and the curly bracket is an anticommutator. In dynamic scaling the Fourier transform of $\tilde{c}^A(r,t)$ is written in the form

$$c^A_\xi(k,\omega) = 2\pi \ \omega^A_\xi(k)^{-1} \ c^A_\xi(k) \ f^A_{k,\xi}\left(\frac{\omega}{\omega^A_\xi(k)}\right)$$

where the subscripts ξ indicate a parametric dependence on the dominant order parameter correlation length. This expression contains the equal time correlation function (t = 0 in (30))

$$c^A_\xi(k) = \int_{-\infty}^{\infty} \frac{d\omega}{2\pi} \, c^A_\xi(k,\omega)$$

and a shape function, f, such that

$$\int_{-\infty}^{\infty} f^A_{k,\xi}(x) \, dx = 1 \quad .$$

The $\omega^A_\xi(k)$ is the characteristic frequency defined by

$$\int_{-1}^{1} f^A_{k,\xi}(x) \, dx = \frac{1}{2} \quad .$$

The shape function, f, is determined by the hydrodynamics of the system being considered. The general relationship between the hydrodynamic equations and correlation functions has been established by Kadanoff and Martin[20], and the specific case of helium has been dealt with in reference 17. The correlation function description is in principle more general than the hydrodynamic description, and the two are equivalent in the limit of small k and ω where hydrodynamics applies. In particular, the

frequencies and damping of the normal modes in hydrodynamics appear as the poles of the appropriate correlation functions. This structure is contained in the shape function, f, given previously. Thus, for example, if the hydrodynamics yields the frequency and damping of a normal mode expressed in terms of the dispersion relation $\omega^2 = u^2k^2 - i\omega k^2 D$ as in equation (27), then the correlation function description of this mode is reflected in a shape function of the type

$$f_{k,\xi}(x) = \frac{1}{\pi} \frac{y_k}{(x^2 - 1)^2 + y_k^2} \quad .$$

The characteristic frequency $\omega_\xi(k)$ implicit in x is just the frequency of the normal mode

$$\omega_\xi(k) = uk \quad ,$$

and the width y_k is

$$y_k = \frac{Dk^2}{uk} = \frac{Dk}{u} \quad .$$

Now one assumption of dynamic scaling is that the shape function for the order parameter correlation function depends on k and ξ only through the product $k\xi$. Thus, if the normal mode and shape function discussed above correspond to that of the order parameter, then this assumption means, since y_k is linear in k, that

$$D \propto u\xi \qquad (31).$$

In the case of the λ-transition there are complications which stem from the fact that the order parameter is the average, over a small region of space-time, of the annihilation field operator[21]. As the field operators are not Hermitian, the order parameter is complex, that is, it has two components. The order parameter correlation function then decays at large r according to a power law, $\bar{p}$, so that

$$c^{\psi}(r) \sim |\psi|^2 \left(\frac{\xi}{r}\right)^{\bar{p}} \qquad \text{for } r \to \infty ,$$

and this serves as a defintion of the correlation length ξ. Also, as demonstrated by the hydrodynamics, there are two propagating modes. However, it is shown in reference 17 that the order parameter correlation function is dominated by the second sound mode to the extent that $(c_p - c_v)/c_p \ll 1$. In addition, it is shown that $c^{\psi}(k,\omega)$, which is not directly observable, has poles which are identical to those of the correlation function of the heat operator

$$\begin{aligned} q(r,t) &= U(r,t) - \frac{\langle U + p \rangle}{\langle p \rangle} \rho(r,t) \\ &= U(r,t) - \langle \mu + T\sigma \rangle \rho(r,t) \end{aligned} \qquad (32).$$

Thus, it is possible to formulate scaling in terms of the observable fluctuations of the heat operator ($\langle dq \rangle \equiv \langle T\rho\, d\sigma \rangle$) which correspond to second sound. The scaling relation (31) is then a prediction of the damping of second sound

$$D_2 \propto u_2 \xi .$$

The significance of this result to this work was discussed in the previous section, B.

iii) Renormalization Group Theory and D_2

The RG treatment of the dynamics of the lambda transition is a work of such magnitude that even a mildly comprehensive development of the prediction for D_2 is beyond the scope of this thesis. Thus, following a discussion of the dynamic model which undergoes the renormalization, only the procedure for performing the RG transformation is indicated. Then the prediction for D_2 is given.

The dynamic models treated by RG techniques are semi-microscopic in

that they are defined by equations of motion for the variables which remain after averaging over length scales which are larger than atomic dimensions but smaller than the correlation length for the order parameter when T is near T_c. One such variable for which an equation of motion must be given is the order parameter, ψ. The equations for the other variables reflect the various symmetries, or equivalently the conservation laws, of the system being studied. In liquid helium there are three conserved fields. As in the two fluid hydrodynamics, they are the energy density, U, the mass density, ρ, and the momentum density, $\vec{j}$. A complete semi-microscopic description of the dynamics of helium would then involve, including the order parameter, four fields. However, it is anticipated that, as a starting point, a two field model is adequate since it is possible to incorporate into such a model the critical hydrodynamic mode associated with a field, m, which couples most strongly to the order parameter. The field m is the linear combination of U and ρ which produces second sound for $T < T_\lambda$ and is denoted by q in equation (32). The two field model of helium is defined by the following stochastic equations[6, 22]:

$$\frac{\partial \psi(x,t)}{\partial t} = -2\Gamma_o \frac{\delta F}{\delta \psi^*} - ig_o \psi \frac{\delta F}{\delta m} + \Theta_n \qquad (33\text{-A}),$$

$$\frac{\partial m(x,t)}{\partial t} = -\lambda_o \nabla^2 \frac{\delta F}{\delta m} + 2g_o \mathrm{Im}\left(\psi^* \frac{\delta F}{\delta \psi^*} \right) + \zeta_n \qquad (33\text{-B}),$$

$$F = F_o - \int d^d x \{ h_m(x,t) m + \mathrm{Re}\left(h_\psi(x,t) \psi^* \right) \} \qquad (33\text{-C}),$$

$$F_o = \int d^d x \{ \tfrac{1}{2} r_o |\psi|^2 + \tfrac{1}{2} |\nabla \psi|^2 + u_o |\psi|^4 + \tfrac{1}{2} c_o^{-1} m^2 + \gamma_o m |\psi|^2 \} \qquad (33\text{-D}).$$

Some of the features of this model are indicated now. The Θ_n, ζ_n are Langevin noise sources. In the absence of time dependent applied fields h_m and h_ψ, these noise sources, when chosen appropriately, ensure that ψ and m achieve values consistent with the equilibrium probability distrib-

ution $P_{eq}(\psi,m) = e^{-F_o(\psi,m)} / \int e^{-F_o(\psi,m)} d\psi dm$. The first three terms in the functional F_o represent the usual Ginzburg-Landau expansion in terms of the order parameter. A similar expansion in the field m is truncated after the first term. In RGT the higher powers of m in the expansion are irrelevant, while in the expansion in powers of ψ the interesting or nontrivial behaviour is a result of the $u_o|\psi|^4$ term. The interaction term, $\gamma_o m|\psi|^2$, in F_o is included because a variation in m, which is identified as second sound, means there is a change in the local value of ΔT which in turn requires that ψ obtain a new local equilibrium value. The first term on the right hand side of (33-A) indicates that ψ is not a conserved field in that it causes ψ to relax ($Re\Gamma_o > 0$) to a value which minimizes F_o. The field m, however, is a conserved quantity since the right hand side of (33-B) can be written as the divergence of a current for $h_\psi = 0$ and ζ_n as given in reference 22.

The significance of the coupling constant g_o in (33-A,B) can be understood by considering the effect of a uniform time-dependent applied field which is conjugate to m, $h_m(x,t) = h_m(t)$. Writing the complex (two component) order parameter in terms of a phase angle ϕ as $\psi = |\psi|e^{i\phi}$, then (33-A) gives the effect of h_m on ϕ as

$$\frac{\partial \phi}{\partial t} = g_o h_m \qquad (34),$$

that is, h_m causes a rotation of the order parameter. Although the notation in (34) is more suggestive of an equivalent system of spins known as the planar ferromagnet[22, 23, 24], the corresponding rotation equation for helium is a "Josephson" equation[21]

$$\hbar \frac{\partial \phi}{\partial t} = \tilde{\mu} \qquad (35)$$

where $\tilde{\mu}$ is the chemical potential per particle of the fluid at rest. The

connection between (35) and the superfluid acceleration equation (5-D) in the two fluid model can be made by the identification $\hbar\vec{\nabla}\phi = \tilde{m}\vec{v}_s$ where $\tilde{m}$ is the mass of a helium atom, and adding the kinetic energy contribution $\frac{1}{2}\tilde{m}\, v_s^2$ to the chemical potential in (35). The result of the coupling, g_o, on the hydrodynamics is that there is a propagating mode for $T < T_c$ which involves coupled variations in m and ϕ[22, 24]. This is second sound in helium while the corresponding mode in the planar magnet is a spin wave.

The renormalization group transformation R_b is applied to the correlation function formulation of the equations of motion (33-A,B,C,D). It is defined by $R_b = R_b^s R_b^i$ where R_b^s is a scale change

$$x \to x' = x/b$$

$$\Lambda \to \Lambda' = \Lambda b$$

$$\psi \to \psi' = b^a \psi$$

$$\omega \to \omega' = b^z \omega$$

such that $b > 1$, and a, z are determined within the theory. The operation R_b^i applied to the diagrammatic expansion of the equations of motion is an integration over wave vectors such that $b^{-1}\Lambda < k < \Lambda$ and frequencies from $-\infty$ to $+\infty$. The transformation is iterated, say n times. The requirement that the equations retain the same form leads to recursion relations for renormalized constants $\{\Gamma_n, g_n, \lambda_n \ldots\}$ which have developed from the original set $\{\Gamma_o, g_o, \lambda_o \ldots\}$. An analysis of the fixed points of the recursion relations, that is, those limiting values $\{\Gamma^*, g^*, \lambda^* \ldots\}$ which remain unchanged by successive iteration, leads to scaling laws as well as values for exponents and certain universal amplitude ratios.

One such universal amplitude ratio is

$$R_2 = \frac{D_2}{2u_2\xi} \tag{36}$$

where D_2 is the damping constant of second sound with velocity u_2, and ξ

is the transverse correlation length of the order parameter. (In superfluid helium there are two correlation lengths, one associated with fluctuations in magnitude, the other with fluctuations in phase. The latter is called the transverse correlation length.) Different methods[14] may be used to evaluate R_2 in three dimensions. One approximation technique using an expansion in $\epsilon = 4 - d$ gives $R_2 \sim 0.15$. Another method is a generalization of RGT to three dimensions and results in $R_2 \sim 0.09$. In each case the calculations are based on the simpler symmetric model for helium (equation (33) with $\gamma_o = 0$) which is expected, in three dimensions, to give the correct asymptotic behaviour as $T \to T_\lambda$. The accuracy for either method of calculation is expected to give R_2 to within a factor of two.

An explicit expression for $D_2(t)$ where $t = (T_\lambda - T)/T_\lambda$ may be obtained by using empirically determined expressions for u_2 and ξ [13]. Ahlers' measurements[9] give $u_2 = 4.63 \times 10^3\ t^{0.387}$ cm/sec at saturated vapour pressure. The same data, in conjunction with the hydrodynamic expression for u_2 and measurements of c_p and σ provide the best information on $\rho_s(t)$. This may be used to evaluate $\xi = \tilde{m}^2\ (k_B T)/\hbar^2 \rho_s(t)$ with the result $\xi = 3.57 \times 10^{-8}\ t^{-0.675}$ cm. Then, the prediction for D_2 becomes

$$D_2 = (\ 3 \text{ or } 5\ ) \times 10^{-5}\ t^{-0.288}\ \text{cm s}^{-1} \qquad (37)$$

depending on the two estimates for R_2. It is noted that both the amplitude and the exponent are subject to verification by experiment.

The recent treatment by Dohm and Folk (DF)[15] of the dynamics of the superfluid transition yields new predictions concerning D_2. They begin with the stochastic model employed by HSH and described by equations 33 A, B, C, D, with $\gamma_o = 0$. However, their analysis of the fixed points of the renormalization group transformation leads DF to predict a temperature dependent effective ratio, $R_2^{\text{eff}}(t)$, which determines D_2 via $D_2/2u_2\xi = R_2^{\text{eff}}$. Using thermal conductivity data above T_λ to evaluate non-universal par-

ameters entering their theory, DF obtain a value for R_2^{eff} at $t = 10^{-4}$ of about 0.14. The temperature dependence is weak over the interval $10^{-4} > t > 10^{-6}$, but stronger for $t > 10^{-3}$. As a simple analytic expression for D_2 is not available in their report, the graphical presentation of their predictions is reproduced in Chapter 4 along with a discussion of the results of this work. They (DF) do not indicate the expected accuracy of their calculations.

CHAPTER 2

EXPERIMENT

The first section of this chapter is a discussion of techniques used in second sound attenuation measurements with particular emphasis on the method chosen for this work. Section B is a discussion of the apparatus. This includes a description of the cryogenic apparatus, the resonator, and the electronics. An outline of the experimental procedure is given in Section C.

A. Techniques

There are several methods available which may be used to measure the attenuation of macroscopic second sound. The most direct approach is that used by Hanson and Pellam (HP). They measure the temperature amplitude, $\tilde{T}$, of a travelling second sound wave as a function of the distance, x, between the generator and detector, and determine the attenuation, α, by means of $\tilde{T} = \tilde{T}_o e^{-\alpha x}$. In another method, as employed by Tyson and Ahlers, the attenuation is determined from the frequency dependence of the amplitude of standing waves in a resonant cavity. A third technique has been developed[25] which involves an analysis of the shape of second sound pulses and has been used to determine the attenuation under pressure but for T much less than T_λ. Other methods are conceivable. For example, one might expect that attenuation measurements could be made using the amplitude decay of a second sound "tone burst" propagating between reflecting plates.

In this experiment a resonance method has been developed in which the attenuation is derived from the decay time, τ, for free oscillations of the plane wave modes of a cylindrical cavity. This is essentially the Fourier transform of the technique used by Ahlers and Tyson. In their experiments

α is related to the full frequency width, $\Delta\omega$, at half maximum of the power, that is, $\tilde{T}^2$, by $\Delta\omega = 2u_2\alpha$. In the present work τ determines the temporal response as $\tilde{T}^2 = \tilde{T}_o^2 e^{-t/\tau}$. The expression which applies to plane travelling waves, $\tilde{T} = \tilde{T}_o e^{-\alpha x}$, becomes $\tilde{T} = \tilde{T}_o e^{-\alpha u_2 t}$ appropriate to a standing plane wave mode and therefore $1/\tau = 2u_2\alpha$. Of course, $\Delta\omega = 1/\tau$. In these expressions α is the total attenuation due to the bulk helium and contributions associated with the boundaries of the resonant cavity.

The decay time method used in this experiment gains one particularly significant advantage while retaining the benefits of a resonance approach. The reasons for choosing a resonance technique in general are based on the desire to approach T_λ as closely as possible and achieve a resolution in ΔT on the order of 10^{-6} K. Thus, in addition to the requirement of temperature stability, a small system is preferred in order to minimize the pressure increase due to gravity which alters the value of T_λ by about 1.3×10^{-6} K per centimeter of helium. It is felt that thermal isolation and small size are more easily achieved with a resonant cavity as opposed to the method of HP which requires a variable propagation path of considerable length to avoid multiple reflections. Also, the effects of finite second sound amplitude (recall the approximations of linearized two fluid hydrodynamics and that $\tilde{v}_n$, $\tilde{v}_s$ are proportional to $\tilde{T}$) become more severe as $T \to T_\lambda$ since then v_s can become large due to the vanishing of ρ_s. Therefore, it is desirable to use small signal levels to avoid what may be a difficult interpretation of large amplitude effects. In addition, the frequency dependence of α_2 indicates that a signal with limited frequency content requires less interpretation than, say, a pulse signal. A resonance method provides a continuous wave, narrow band signal to which standard but powerful detection techniques may be applied. Moreover, the resonance itself results in an amplification of the AC excitation. This

is important if the second sound is generated, as it is in this experiment, by the AC electrical heating of a resistive element. Then there is a DC component present in the power spectrum of the excitation which results in a steady counterflow of v_n and v_s upon which the AC second sound flow is superimposed. However, to the extent that the 'gain' of the cavity is very large, the DC flow velocities are negligible in comparison to the AC flow velocities. As this selective 'gain' is not present in the methods using a travelling wave, or pulsed second sound, a resonance method is preferred since it is expected that with a DC counterflow there are corrections to the expression (27) for the attenuation[18].

The measurement of decay times as opposed to line widths overcomes a problem related to the limitations of temperature stability and frequency range that are encountered in this experiment. To understand the nature of the problem, consider the harmonic sequence for plane-wave modes in a cavity consisting of parallel plates separated by a length a. The resonant frequencies are given by

$$\omega_p = u_2 k_p = u_2(p\pi/a)$$

where p = 1, 2, 3 ... . During the course of a frequency sweep through some resonance of width $\Delta\omega_p$ at ω_p suppose that the ambient temperature changes by δT. Then the second sound velocity changes by $\delta u_2 = (\partial u_2/\partial T)\delta T$ and, therefore, the resonant frequency changes by an amount $\delta\omega_p = \delta u_2 k_p$, or $\delta\omega_p = (\delta u_2/u_2)\omega_p$. For small ΔT, δu_2 becomes large since $\partial u_2/\partial T$ diverges as $T \to T_\lambda$. The amplitude response to the driven oscillations now approaches a different value appropriate to the new resonant frequency $\omega_p + \delta\omega_p$. Thus, the typical temperature fluctuations, δT, result in distortions of the resonance response curve making it difficult to determine $\Delta\omega_p$. This is significant when the "temperature noise width", $\delta\omega_p$, becomes comparable

to the intrinsic width $(\Delta\omega_p)_{\alpha_2}$. In principle this problem can be overcome by using higher harmonics since the intrinsic width is expected to vary as $(\Delta\omega_p)_{\alpha_2} = 2u_2\alpha_2 = (\omega_p^2/u_2^2)D_2$, and the frequency squared dependence will ultimately dominate the linear dependence in $\delta\omega_p = (\delta u_2/u_2)\omega_p$. Unfortunately, modes which do not correspond to plane waves, but rather to Bessel functions, complicate the cavity response. The excitation of 'Bessel modes', to be discussed below, makes it difficult in this experiment to interpret the resonant structure at the frequencies of the higher harmonics. However, the attenuation, α_2, can be obtained by measuring the decay times of the well isolated, low frequency harmonics. In this method the cavity is driven at or near the resonant frequency until the excitation reaches some desired high level. The drive is then turned off and the decay of the excitation recorded. The oscillation frequency still fluctuates by $\delta\omega_p$ due to the temperature noise, δT, but now this does not appear as amplitude noise in the signal since the response is not driven but allowed to decay freely. It is only necessary that the bandwidth of the detection system be large enough to accommodate the frequency content of the decay, $e^{-t/\tau}$, and the excursions, $\delta\omega_p$, which occur during the decay. The details of the signal recovery system are found in the discussion of the electronics.

The general resonant frequencies of a cylindrical cavity of radius r and length a are given by.[26]

$$\omega_{p,m,n} = \pi u_2 \left(\left(\frac{p}{a}\right)^2 + \left(\frac{\alpha_{mn}}{r}\right)^2 \right)^{\frac{1}{2}} \qquad (38).$$

The α_{mn}, with m, n = 0, 1, 2 ... , are solutions to $\{dJ_m(\pi\alpha)/d\alpha\} = 0$, where $J_m(\pi\alpha)$ is a Bessel function of the first kind. The plane wave modes are obtained for $\alpha_{00} = 0$. The modes with m or n not zero are loosely referred to as Bessel modes. For m or n near one, the α_{mn} are on the order of unity, while for large m and n approximate values are $\alpha_{mo} \simeq m/\pi$ and

$\alpha_{mn} \simeq n + \frac{1}{2}m + \frac{1}{4}$ when $n > m$. The dimensions of the cavity in this experiment are such that $r \simeq 2.4\ a$, and therefore the lowest resonant frequencies correspond to Bessel modes. The density of the Bessel modes increases with frequency with the result that at the frequencies of the higher plane wave harmonics there may be several Bessel modes having nearly the same frequency as any particular plane wave mode. With the use of equation (38) and the tabulated[26] values of α_{mn} for $m = 0$ to 8 and $n = 1$ to 20, the resonant frequencies can be calculated to determine which of the plane wave modes are well separated from Bessel modes. Because of the high density of the Bessel modes, the results are sensitive to the value of the ratio r/a, which is known with an accuracy of about ± 0.5%. In anticipation of the observations on harmonics 1, 2, 3 and 4, a calculation indicates that the first and third harmonics are isolated to the extent that to within ± 1% of their frequencies there are no Bessel modes. In view of the uncertainty in r/a, this means that harmonics one and three are fractionally isolated from Bessel modes by at least 0.5% of their respective frequencies. This degree of isolation is significant since it is large compared to the maximum fractional width of a resonance, $\Delta\omega/\omega_p$, of about 0.05%. However, for harmonics two and four, there are two Bessel modes within ± 0.5% of the frequency of harmonic two, and four in the case of harmonic four. Thus, if the Bessel modes are excited, they could influence the response at the second and fourth harmonics. The consequences of the position of the Bessel modes will be discussed in more detail in relation to the experimental observations. Possible mechanisms which may be responsible for the excitation of the Bessel modes are suggested in the general discussion of the concluding chapter.

B. Apparatus

I) Cryogenic Apparatus

The general features of the cryogenic apparatus are illustrated in Figure 1 and described here. The experimental cell containing the resonator was suspended inside an evacuated container. This in turn was immersed in a bath of liquid helium ($T < T_\lambda$) to provide a stable thermal environment. The temperature of this outer bath could be regulated[27] to better than 10^{-4} K over a half hour interval. Helium from this bath filled the experimental cell (about 15 cm^3) through a valve and capillary. A porous stainless steel filter over the valve entrance kept solid air particles out of the capillary and valve seat. An estimate of the helium level in the cell was made using a depth gauge that consisted of a cylindrical capacitor that formed part of a tunnel diode oscillator. A thermometer and standard resistor at the bottom of the cell formed the cryogenic part of a bridge circuit that was primarily used as a temperature controlling device in conjugation with a feedback resistor wound on the outside of the copper top of the cell body. The second sound resonator was held in a brass frame that enabled the resonator body to be held together by spring loading. The second sound detector (bolometer) in the resonator was a superconducting device. Its transition temperature was trimmed to the desired temperature by a magnetic field produced by means of a solenoid wound on the outside of the vacuum container.

A few other features might also be considered as follows:

(i) A second capillary connected the cell to room temperature access. This was available for pumpimg away excess helium in case of accidental overfilling. Also, this line would be necessary for studies at elevated pressures.

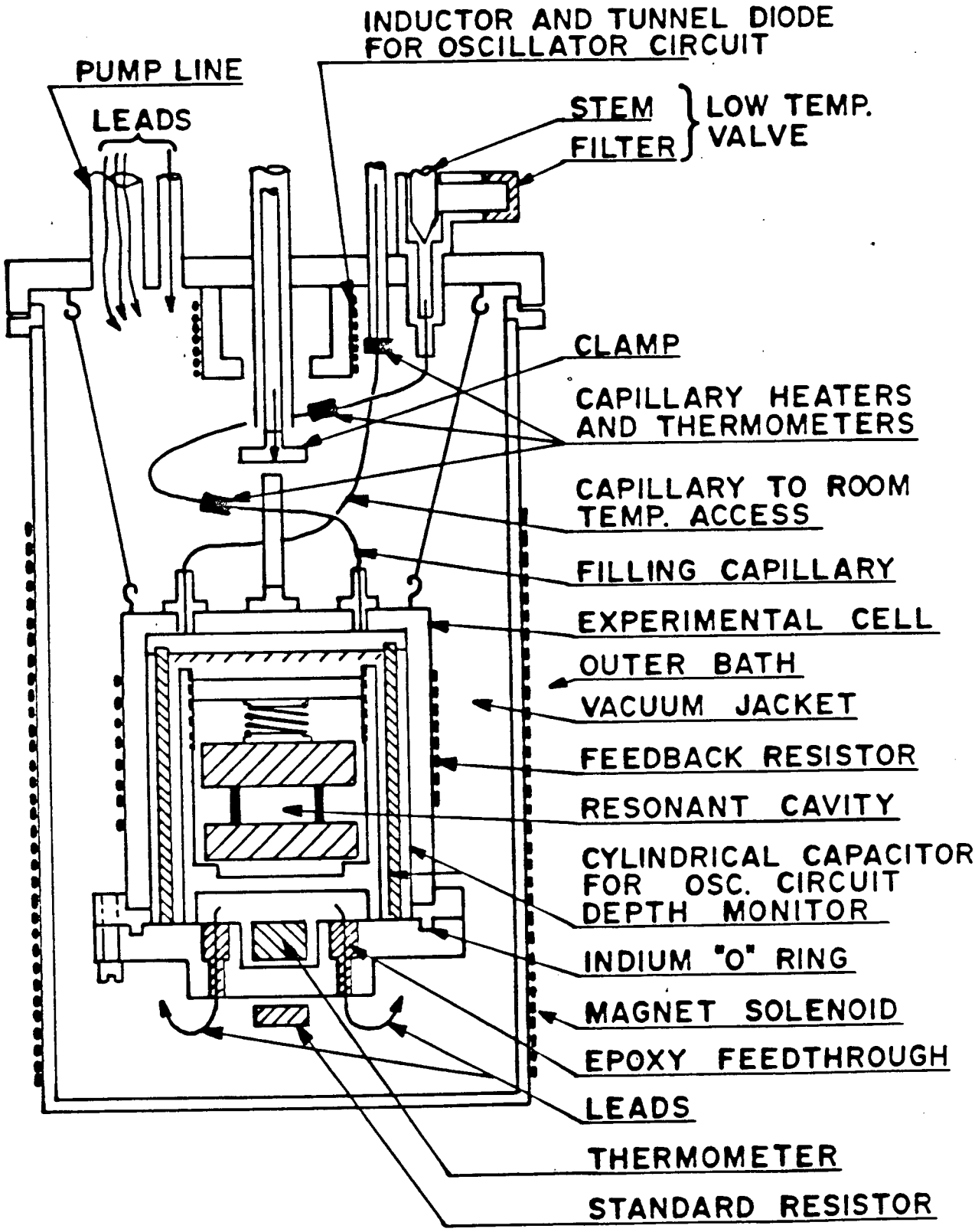

Figure 1

Cryogenic Apparatus

(ii) There existed several thermometers and heaters at various locations that were used to establish initial working conditions. Those mounted on the capillaries were particularly important since it was necessary to destroy temperature instabilities of an oscillatory character, and magnitude of about 10^{-3} K, that were generated by helium in the capillaries. The insertion of piano wire (0.2 mm diameter wire in 0.3 mm i.d. capillary) along with the power input from the heaters overcame these instabilities.
(iii) The cell, suspended by three steel piano wires, was held secure by using the remnants of a poorly designed heat switch as a clamp.
(iv) General purpose electrical leads made of Advance alloy were brought down the vacuum pumping line. Signal leads for the bolometer, generator, thermometer and level indicator were brought down separate stainless steel tubes. The bolometer leads consisted of a twisted pair of #40 copper wire. Leads into the cell were brought through holes in the bottom brass flange and sealed with epoxy.

II) Resonator

(i) Cavity

A side view of the resonator is shown in Figure 2a. Two fused quartz optical flats separated by a stainless steel annulus (length 3.0 mm, inside radius 7.4 mm, and wall thickness 0.38 mm) formed the cylindrical resonant cavity. Thin ($\sim 6 \times 10^{-3}$ mm) mylar gaskets glued to the annulus electrically isolated the bolometer and generator thin films on the flats from the annulus. Polishing the ends, with gaskets in place, ensured that the flats (better than one light wave flat) were parallel to within a few light waves. It was hoped that this alignment would result in preferential excitation of only plane wave modes. The inside surface of the annulus was also polished. After assembly a small amount of glycerine was applied to

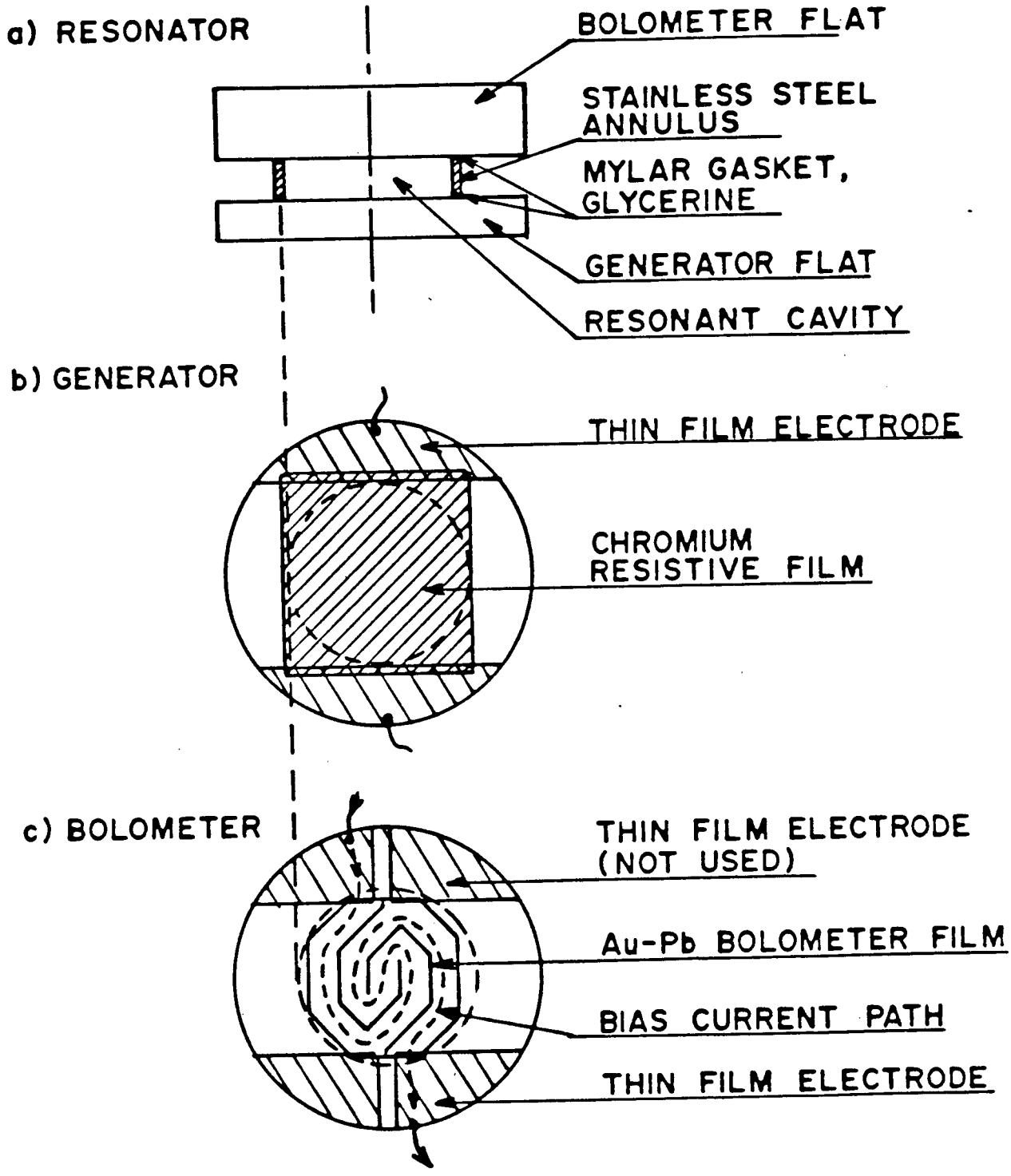

Figure 2

The Resonator, Generator and Bolometer

the corners formed by the annulus and flats. This ensured that the cavity interior was sealed off from the external helium in the cell and prevented any possible coupling between the internal cavity modes and those modes that existed outside. Such a coupling could result in an energy loss mechanism that might be misinterpreted as intrinsic attenuation. However, it was still possible for the superfluid to penetrate the gylcerine seal and fill the resonator in approximately four hours.

The optical flats, with 25 mm diameter, were typical of those commercially available. They were quite thick, the flat with the generator being 3.2 mm while the one with the bolometer was 6.4 mm thick. Both materials, fused quartz glass and stainless steel, used in the construction of the cavity have low thermal conductivities. This property resulted in strong reflection of the second sound at the boundaries and will be discussed in more detail in following chapters. The heat generated in the cavity escaped mostly through the relatively thin annulus walls and raised the temperature of the cavity by about 20 KW^{-1} above the ambient temperature of the cell.

Considerable effort went into the construction of the thin resistive films which constitute the bolometer and generator. Besides possessing specific properties described below, it was felt that they should be as close as possible to an ideal surface so that "perfect" reflection occurred at the end plates. Indeed, recent studies[28] comparing thin resistive films (Aquadag) to superleak (nucleopore) transducers have indicated that the reflection properties of the former are much simpler to interpret.

(ii) Generator

A top view of the generator is shown in Figure 2b. Conventional vapour deposition techniques have been used in construction. The parallel strip

electrodes were deposited first. Particularly robust electrodes were made by depositing a thin layer of chromium with a film of gold on top. Simpler, less expensive but less durable electrodes were also made using only aluminum. Electrodes were typically 300 nm thick with a resistance less than 1 Ω per square. Leads of #40 copper wire were usually attached by simply cold welding with a bit of indium. The active resistive element which generated the second sound was a thin uniform film of chromium overlapping the electrodes at the edges. The resistance of this film was about 43 Ω per square, independent of temperature from 300 K to 2 K. Its thickness has not been determined accurately, but the resistance would indicate that it was at least 3 nm, while mechanical measurements gave an upper limit of about 100 nm. The film was sufficiently robust that it suffered no damage on contact with the annulus. The position and size of the annulus relative to the generator are indicated by the dashed circle in Figure 2b.

The reason for choosing the geometry illustrated in Figure 2b was to preferentially excite the plane wave modes of the cavity. The significance of the thickness, d, of the generator film can be appreciated by comparing it to the length $\delta = (2D/\omega)^{\frac{1}{2}}$ which governs the phase and exponential attenuation of temperature oscillations at angular frequency ω in a material of diffusivity D [29]. The diffusivity ($D = \bar{\kappa}/\bar{c}$ where $\bar{\kappa}$ is the thermal conductivity and $\bar{c}$ is the specific heat per unit volume) is difficult to estimate for what is probably a polycrystalline chromium film; however, even a cautious estimate indicates that $d \ll \delta$ for the frequency range of this experiment. This means the generator was thin in a thermal sense. Therefore it was capable of fast response, and the reflection properties were determined by the glass substrate.

(iii) Bolometer

The temperature sensitive mechanism of the bolometer was the superconducting transition of a gold and lead composite film[30]. The center temperature of transition was adjusted, by means of a magnetic field, to the operating temperature of the resonator. The temperature excursions associated with second sound resulted in corresponding variations in the resistance of the film. By biasing the film with a constant current the resistance variations appeared as voltage changes which in turn were recovered by the electronics.

The gold-lead films were constructed by depositing 8.0 nm of gold followed by 14 nm of lead[31]. The gold was evaporated from a tungsten filament, the lead from a boat or crucible lined with Al_2O_3. Deposition rates were 10^{-1} nm per second. The films were extremely delicate and sensitive to chemical attack when left exposed to the atmosphere for periods of about a day. The resistance of the films at room temperature was about 25 Ω per square. The superconducting transition was typically 5×10^{-2} K above T_λ, and could be lowered to T_λ by a field of about 100 gauss.

The electrode and bolometer configuration are shown in Figure 2c. Apart from the difference in pattern, the electrodes are similar to those used in the generator. The operating resistance of a square section of film was too low to provide an adequate signal level and impedance match to the electronics. To remedy this, the resistance of the bolometer was increased by a factor of 20 by cutting it with a steel scribe into the pattern shown in the figure. A typical current path for the constant bias is shown by the dotted line. This particular pattern was chosen to maintain an active area as large as possible without allowing the easily damageable films to come into contact with the annulus. The sides of the

film were also cut to prevent edge effects from reducing the sharpness of the transition.

A useful figure of merit for a bolometer of resistance R is the sensitivity defined by (1/R)(dR/dT). For the bolometer used in this work the most rapid variation of R with T occurred near the center of the transition where R had fallen to one-half the high temperature value. There the resistance and sensitivity were 140 Ω and 40 K^{-1} respectively. As a comparison, the sensitivity of conventional carbon film bolometers is more than a factor of ten smaller.

The bolometer film was also thermally thin and capable of fast response. However, it might be expected that the power dissipation due to the bias current would have some effect on the resonance decay, and consideration was given to this in the collection of data.

III) Electronics

A block diagram of the major electronic circuitry is shown in Figure 3.

(i) Signal Excitation and Recovery

The output, at f/2, of a frequency synthesizer[32] was supplied to the generator which produced, by Joule heating, second sound at frequency f. The same f/2 output served as a reference for the lock-in analyzer[33]. The cavity response signal, as detected by the bolometer, was amplified[34] and fed to the lock-in analyzer which responded to the second harmonic of the original f/2 reference. The outputs available from the analyzer were the components of the signal that were in-phase, I, and out-of-phase, Q, with respect to the reference. These components were squared[35] and summed to produce a signal, $I^2 + Q^2$, which was proportional to the squared amplitude of the second sound in the cavity. In the measurement of decay times, once

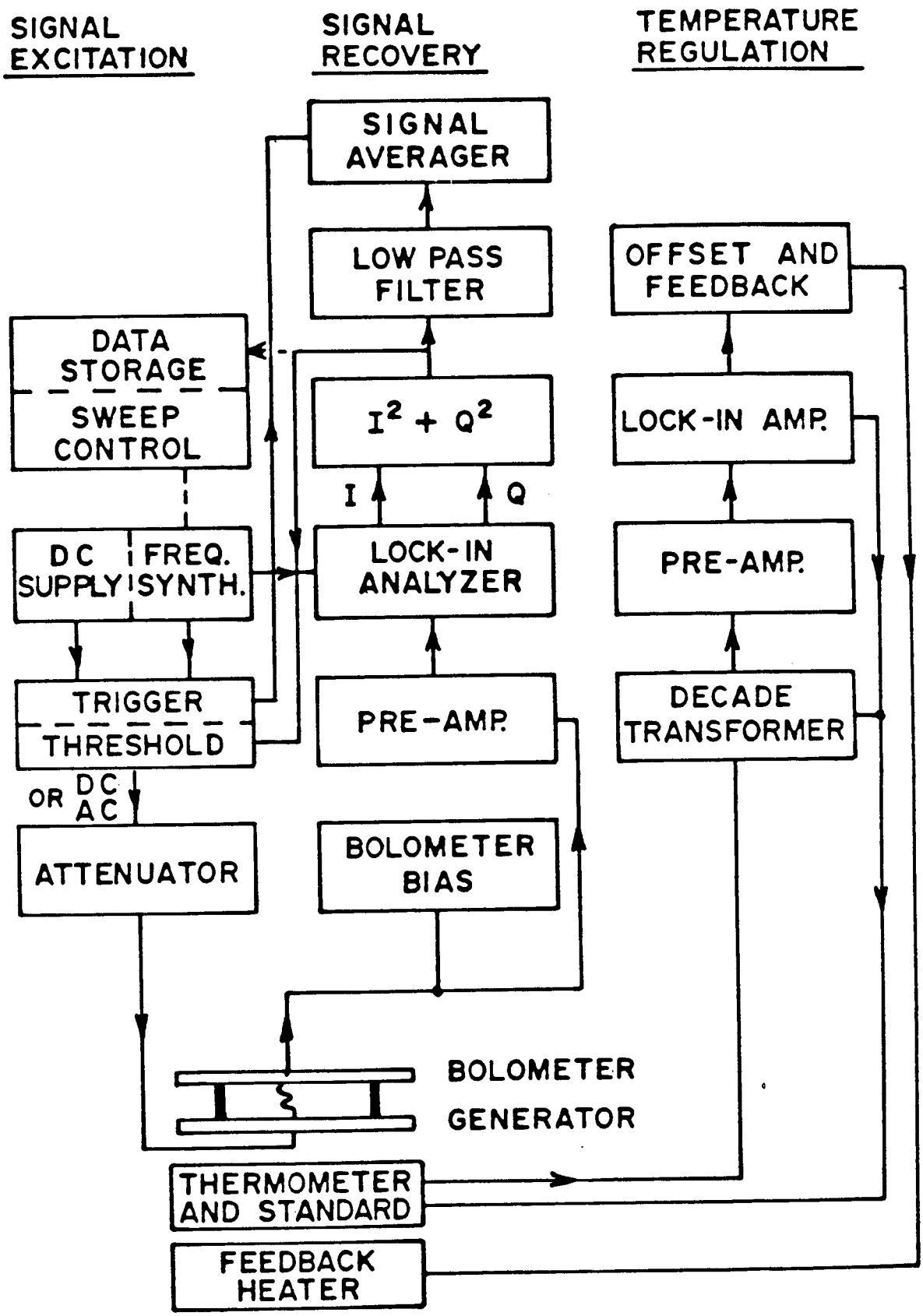

Figure 3

Block Diagram of Main Electronics

the $I^2 + Q^2$ signal reached some preset threshold the AC excitation to the generator was interrupted and replaced with a DC drive which produced equivalent power input to the resonator. This enhanced the temperature stability in the cavity. Simultaneous with this inerruption, a pulse was sent to trigger the signal averager[36] and the decay of the $I^2 + Q^2$ signal was recorded. After some predetermined time the AC excitation was again applied to the generator. If the resonant frequency of the cavity had changed slightly due to temperature drifts then the frequency of the synthesizer was manually adjusted by some acceptable small amount to come back onto resonance. The process was repeated until, by averaging, an acceptable signal to noise ratio was achieved.

As previously mentioned, it was necessary that the bandwidth of the detection system be sufficiently wide to accommodate the frequency excursions of the signal during decay, as well as the frequency content of the decay. This requirement strictly applied in the initial filtering stages where the narrow bandwidth appeared at the lock-in analyzer. However, following the square and sum operation it was useful to insert a low pass filter. Since at this stage it was only necessary to pass the decay signal, the "bandwidth" of this filter could sometimes be less than that of the lock-in analyzer.

Initially it was useful to identify the mode structure of the cavity by recording the response as a function of the drive frequency. Then the threshold device and signal averager were not active. A microcomputer stepped the synthesizer and stored the cavity response at each frequency increment. The resulting data could be readily plotted using the U.B.C. computing facilities.

(ii) Temperature Regulation

The internal reference of a lock-in amplifier was used to excite a bridge circuit consisting of a seven decade ratio transformer[37] and two cryogenic arms containing a carbon resistance thermometer and a temperature insensitive reference resistor. The amplified[38] unbalanced signal from the bridge was fed to the lock-in amplifier[39], the output of which was combined with a DC offset and then applied[40] to the heater wound on the experimental cell. This negative feedback maintained a null signal and regulated the temperature of the cell at a value corresponding to the bridge ratio. With this control scheme the balanced bridge ratio could be held fixed for several hours to within the low frequency (0.2 Hz) temperature noise of $\pm 2 \times 10^{-6}$ K. From the measured sensitivity of the system, different values of ΔT could be obtained by simply changing the bridge ratio to the appropriate value.

(iii) Level Detection

This circuit if not shown in Figure 3. Essentially it was an oscillator consisting of an LC circuit driven by a tunnel diode[41]. The level sensing component was the capacitance formed by a tube and the inside of the cell (see Figure 1). The accuracy of this device, ± 10% of full, was limited by the mechanical stability of the entire cryostat. Nevertheless, it was found extremely useful during filling, and permitted a daily check on the level in the cell.

C. Procedure and Tests

Initial studies were performed at large values of ΔT ($\Delta T > 2 \times 10^{-2}$K) to determine which modes of the cavity were excited and, in particular, to search for plane wave modes which were well separated from other Bessel modes. By sweeping the frequency through the plane wave modes it was

found that the first and third harmonics were "clean", while the other harmonics were accompanied by the nearby resonant structure of Bessel modes. Similarly, the time decay of the first and third harmonics was governed by a single time constant, while the other harmonics displayed a more complicated behaviour where beating with the nearby resonances was often evident. Consequently, the time decays of harmonics one and three were obtained for smaller values of ΔT. The data covered the temperature range $4 \times 10^{-5} \lesssim \Delta T \lesssim 5 \times 10^{-2}$ K, over which the frequency of the fundamental harmonic varied from 112 to 1,730 Hz.

At each temperature several decay curves were recorded for different values of both the bolometer bias power and the amplitude of the second sound in the cavity. The effects of bolometer power, which ranged from 3.6×10^{-7} W to 2.5×10^{-6} W, were usually weak. Amplitude effects, however, could be quite severe in that there was a critical amplitude above which a resonance would decay very quickly with a strong amplitude dependence. Below this critical value the decay rate was much slower, although there still remained a weak amplitude dependence that became more significant as $T \to T_\lambda$. To stay below the critical amplitude, which became smaller for decreasing ΔT, it was necessary to use second sound with initial (i.e. at the beginning of a decay) temperature amplitudes as low as 3×10^{-8} K rms. The recovery of these signals required averaging over hundreds of decays. The final results derived from the data for the first and third harmonics at fifteen values of ΔT are determined from the analysis of 250 decay curves, each representing an average of between 16 and 450 decays. The minimum generator power density used to excite the cavity was as low as 3×10^{-9} W cm^{-2} and 1×10^{-8} W cm^{-2} for the first and third harmonics respectively, while for large ΔT levels as high as $\sim 10^{-6}$ W cm^{-2} were used to study amplitude effects. The treatment of the

residual amplitude and power dependence is discussed in the analysis of results.

The temperature difference, ΔT, was determined using the expression[9, 42] for the second sound velocity

$$u_2 = 46.28(\Delta T/T_\lambda)^{.387} \text{ m s}^{-1}, \tag{39}$$

and the observed resonant frequency, f_1, of the fundamental harmonic which gives u_2 by

$$u_2 = 2af_1$$

where a is the known length of the resonator. This method, as opposed to measurements with the thermometer, was used because it gave a value of ΔT appropriate to the interior of the cavity which was at a temperature typically 2×10^{-5} K greater than the surrounding bath which contained the thermometer. Also, it eliminated the need for the tedious, periodic calibration of the thermometer which is known[43] to drift slowly with time. The validity of the procedure to derive ΔT from f_1 via u_2 was checked once by calibrating the thermometer at the lambda-point using the anomaly in the warming curve[43]. A value of $\Delta T \sim 4 \times 10^{-5}$ K derived from this calibration point and the measured[44] thermometer sensitivity ($1/R(dR/dT) = 1.27\ K^{-1}$) was consistent with that derived on the basis of second sound velocity and the estimate of the internal heating in the cavity. For $\Delta T > 2 \times 10^{-2}$ K the expression (39) begins to break down and a simple graphic interpolation of the numerical data given by Ahlers[9] was used to determine $u_2(\Delta T)$.

While collecting data, the drifting thermometer calibration resulted in a corresponding change in the value of ΔT and resonant frequency for a fixed value of the bridge ratio. This was compensated for by adjusting the bridge setting appropriately to maintain a fixed ΔT within suitable

limits, typically $\pm$ 2 x 10^{-6} K.

The uncertainty in ΔT is the maximum of $\pm$ 3 x 10^{-6} K or $\pm$ 0.5% of ΔT. The major contributions to this error estimate are the uncertainty in the cavity length, a, which enters the above expression for u_2, and the stability in ΔT during the collection of data. It will be evident in the presentation of results in Chapter 4 that this uncertainty in ΔT is insignificant in comparison to the error estimates on the damping.

During the collection of data it was realized that a thermal emf ($\sim$ 3 x 10^{-3} V) resulted in a dissipation of about 10^{-7} W in the generator. This power was eliminated by using a simple battery circuit to oppose the current driven by the emf. Studies indicated the the thermo-electric power had no effect on the decay curves for the first and third harmonics. However, when the thermal emf is added to the AC voltage excitation at frequency f, the resulting power spectrum has a contribution at f, as well as the desired 2f component. Thus, when exciting an even numbered harmonic at 2f there would also be present the harmonic at f. In the case of harmonics two and four, it was found that the nearby resonant structure disappeared when the thermo-electric power, and consequently the coincidental excitation of harmonics one and two respectively, was eliminated. Therefore, with the thermo-electric power absent, some data was collected on the second and fourth harmonics. However, as will be discussed in the analysis of results, for these resonances there still appears to be some additional loss that is probably related to the existence of the nearby modes that were evident when the two harmonincs, four and two, or two and one, were simultaneously excited.

CHAPTER 3

INSTRUMENTAL SOURCES OF ADDITIONAL ATTENUATION

This chapter contains a discussion of sources of attenuation of second sound other than that arising from the bulk helium. These additional sources of energy loss occur at the boundaries of the resonator and result from thermal conduction and the viscosity, η, of the normal fluid. The total attenuation, α, is written as

$$\alpha = \alpha_2 + \alpha_\eta + \alpha_e + \alpha_s$$

where α_2 is the bulk contribution given by equation (28) on page 15, α_η is the contribution from viscous drag at the side walls, α_e and α_s result from thermal conduction at the reflecting end plates and side walls respectively. The development of the expression for α_η has been presented in considerable detail by Heiserman and Rudnick[45], while the thermal conduction losses have been treated by Khalatnikov[46]. The derivations of the expressions for α_η, α_e, α_s are outlined in sections A and B. Some aspects of the application of these results to this experiment are discussed in section C.

A. Attenuation Due to Viscous Surface Loss, α_η

For a plane wave of second sound propagating in a tube, the normal fluid, which moves parallel to the wall of the tube, is entrained in the vicinity of the wall due to viscous interaction. This effect penetrates into the fluid a characteristic distance $\lambda = (2\eta/\rho_n\omega)^{\frac{1}{2}}$ and results in a velocity dispersion and attenuation. This expression for λ is obtained from the related problem of an oscillating plate in contact with a viscous fluid. In that case the solution[18] is a viscous diffusion wave with λ determining the normal fluid velocity a distance x from the plate by

$$v_n = v_{no} e^{-x/\lambda} e^{-i(\omega t - x/\lambda)}.$$

To calculate the viscous surface losses for second sound propagating along a tube of cross-sectional area A and perimeter B, the linearized two fluid hydrodynamic equations of Chapter 1 are employed. Again, using δ to denote small quantities, the non-dissipative equations for mass, entropy, and superfluid acceleration are:

$$\partial\delta\rho/\partial t + \nabla\cdot(\rho_n \delta\vec{v}_n + \rho_s \delta\vec{v}_s) = 0 \qquad (40),$$

$$\rho(\partial\delta\sigma/\partial t) + \sigma(\partial\delta\rho/\partial t) + \rho\sigma(\nabla\cdot\delta\vec{v}_n) = 0 \qquad (41),$$

$$\partial\delta\vec{v}_s/\partial t = -\nabla\mu \qquad (42).$$

The linearized momentum equation, which is $\partial(\rho_n\delta\vec{v}_n + \rho_s\delta\vec{v}_s)/\partial t = -\vec{\nabla}p$ in the non-dissipative approximation, is modified to include the effects of viscous interaction with the walls. Choosing the z-axis as the propagation direction and denoting by r the perpendicular coordinate which is zero at the wall, the momentum conservation law including a viscous stress term is

$$\frac{\partial(\rho_n\delta v_{nz} + \rho_s\delta v_{sz})}{\partial t} = -\nabla p - \frac{B}{A}\eta\frac{\partial v_{nz}}{\partial r}\Big)_{r=0} \qquad (43).$$

The assumption implied in writing this equation is that the viscous penetration length is much smaller than the lateral dimension of the tube and, therefore, the wave fronts are essentially plane wave. The approximation is valid for this experiment since λ is typically 10^{-3} to 10^{-4} cm.

For a second sound wave the fluid momentum is zero[16, 18], that is,

$$\rho_n v_n + \rho_s v_s = 0 \qquad (44).$$

Thus, the hydrodynamic equations become

$$\partial\delta\rho/\partial t = 0 \qquad (45),$$

$$\partial\delta\sigma/\partial t = -\sigma\partial v_{nz}/\partial z \qquad (46),$$

$$\partial \delta v_{sz}/\partial t = +\sigma(\partial T/\partial z) - 1/\rho(\partial p/\partial z) \qquad (47),$$

$$\partial p/\partial z = -(B/A)\eta\,(\partial \delta v_{nz}/\partial r)\big|_{r=0} \qquad (48).$$

With equations (44, 46, 47, 48) and the approximation $\partial T/\partial z \sim (T/c)\partial\sigma/\partial z$ which neglects $(\partial T/\partial p)_\sigma$ for second sound, it is easy to derive the following wave equation for the entropy:

$$\frac{\partial^2 \delta\sigma}{\partial t^2} + \frac{\rho_s}{\rho\rho_n}\frac{B}{A}\eta\ \frac{\partial^2 \delta\sigma}{\partial t \partial r}\Big|_{r=0} = u_2^2 \frac{\partial^2 \delta\sigma}{\partial z^2} \qquad (49)$$

where $u_2 = (\rho_s T\sigma^2/\rho_n c)^{\frac{1}{2}}$ is the speed of second sound. By analogy to the oscillating plate problem, a solution to (49) is attempted in the form

$$\delta\sigma = \delta\sigma_o(1 - e^{ir/\lambda - r/\lambda})\, e^{i(k'z - \omega t)} \qquad (50)$$

with $k' = k + i\alpha_\eta$. Substituting (50) into (49) gives

$$\omega^2\delta\sigma + i\omega\frac{\rho_s}{\rho\rho_n}\frac{B}{A}\frac{\eta}{\lambda}(1 - i)\delta\sigma_o e^{i(k'z - \omega t)} = u_2^2 k'^2 \delta\sigma \qquad (51).$$

Now, for λ much smaller than the lateral dimensions of the tube, the approximation $\delta\sigma \simeq \delta\sigma_o e^{i(k'z - \omega t)}$ is made in (51) with the real and imaginary components resulting in

$$\omega^2 + \omega(\rho_s/\rho\rho_n)\ (B/A)(\eta/\lambda) = u_2^2(k^2 - \alpha_\eta^2)\ ,$$

and

$$\omega(\rho_s/\rho\rho_n)(B/A)(\eta/\lambda) = 2u_2^2\,\alpha_\eta k\ .$$

Solving these equations yields the dispersion $\omega(k)$ and, for small dispersion where $\omega \simeq u_2 k$, the attenuation:

$$\alpha_\eta = \frac{1}{2u_2}\left(\frac{B}{A}\right)\frac{\rho_s \eta}{\rho\rho_n\lambda}\ .$$

Using $\lambda = (2\eta/\rho_n\omega)^{\frac{1}{2}}$, then the viscous surface attenuation for a circular cylinder of radius r, as in this experiment, is:

$$\alpha_\eta = (1/ru_2)(\rho_s/\rho)(\eta\omega/2\rho_n)^{\frac{1}{2}} \qquad (52).$$

B. Attenuation Due to Heat Conducting Surface Losses, α_e and α_s

The temperature excursions associated with second sound result in thermal conduction at the boundaries which diminishes the magnitude of the temperature excursions and, therefore, contributes a source of attenuation.

Neglecting dissipation in the helium, consider a plane wave of second sound propagating in the z-direction and incident on a solid body filling the half space $z > 0$. In the second sound wave the energy flow, $\mathcal{J}$, in the z direction through unit area per unit time is written as

$$\mathcal{J} = (\mathcal{J}_1 e^{ikz} - \mathcal{J}_2 e^{-ikz}) e^{-i\omega t} \tag{53}$$

where $\mathcal{J}_1$ and $\mathcal{J}_2$ are the amplitudes in the incident and reflected waves respectively. The corresponding temperature oscillations, $\mathcal{T}$, are given by

$$\mathcal{T} = (1/\rho c u_2)(\mathcal{J}_1 e^{ikz} + \mathcal{J}_2 e^{-ikz}) e^{-i\omega t} \tag{54}$$

with c being the specific heat of helium. The desired quantity to be calculated is the reflection coefficient $\mathcal{J}_2/\mathcal{J}_1$. At the boundary there are two thermal impedances to be considered, one being the impedance of the solid body, the other is the Kapitza resistance of the surface itself. The profile of the temperature excursions, T', in the solid body is determined by the heat equation

$$\bar{c}(\partial T'/\partial t) = \bar{\kappa}(\partial^2 T'/\partial z^2) \tag{55}$$

where $\bar{\kappa}$ is the thermal conductivity, and $\bar{c}$ is the heat capacity per unit volume of the solid. The solution to (55) with the boundary condition $T'(z=0) = T'_o e^{-i\omega t}$, is the diffusion wave

$$T' = T'_o e^{-\sqrt{\bar{c}\omega/\bar{\kappa}}\,(1/\sqrt{2} - i\sqrt{2})z}\, e^{-i\omega t} \tag{56}.$$

The amplitude of the temperature excursions, T'_o, of the wall at $z = 0$ is not equal to the amplitude, $(\mathcal{J}_1 + \mathcal{J}_2)/\rho c u_2$, in the helium at $z = 0$ due to the Kapitza resistance, 1/G, of the surface. The requirement of contin-

uity of energy flow at the boundary provides two equations:

$$\mathcal{J}_1 - \mathcal{J}_2 = G\{(\mathcal{J}_1 + \mathcal{J}_2)/\rho c u_2 - T_o'\} \tag{57}$$

and

$$(\mathcal{J}_1 - \mathcal{J}_2)e^{-i\omega t} = -\kappa \mathrm{Re}\{\partial T'/\partial z)_{z=0} \tag{58}.$$

Implicit in writing (58) is an approximation which neglects in (53) a small contribution to $\mathcal{J}_2$ of magnitude $\mathcal{J}_1 - \mathcal{J}_2$ and phase shifted by $\pi/2$ with respect to $\mathcal{J}_2 e^{-i\omega t}$. Substituting (56) into (58), and eliminating T_o' from (57) and (58), gives

$$\frac{\mathcal{J}_2}{\mathcal{J}_1} = \frac{1 - \dfrac{(G/\rho c u_2)}{1 + G(2/\bar{c}\bar{\kappa}\omega)^{\frac{1}{2}}}}{1 + \dfrac{(G/\rho c u_2)}{1 + G(2/\bar{c}\bar{\kappa}\omega)^{\frac{1}{2}}}} \tag{59}.$$

Using the inequality $G \ll \rho c u_2$, which holds for the temperature range of this experiment, the reflection coefficient becomes

$$\frac{\mathcal{J}_2}{\mathcal{J}_1} = 1 - \frac{2}{\rho c u_2 (1/G + \sqrt{2/\bar{c}\bar{\kappa}\omega})} \tag{60}.$$

Although there is considerable variation (an order of magnitude) in the reported measurements of the Kapitza resistance near T_λ, for the largest frequencies in this experiment the solid body resistance, $\sqrt{2/\bar{c}\bar{\kappa}\omega}$, is greater than the Kapitza resistance. The approximation which neglects 1/G, to be discussed in section C of this chapter, yields for the reflection coefficient

$$\mathcal{J}_2/\mathcal{J}_1 = 1 - \beta = 1 - (2/\rho c u_2)\sqrt{\bar{c}\bar{\kappa}\omega/2} \tag{61}.$$

This result is now used to calculate the attenuation, α_e and α_s, due to thermal conduction at the ends and side walls of the resonant cavity.

Consider a plane wave propagating between reflecting end plates separated by a distance 'a'. It is evident that the effective attenuation, α_e, due to reflection is such that $e^{-\alpha_e a} = 1 - \beta$. Substituting from (61),

and using $\beta << 1$, gives

$$\alpha_e = \frac{2}{a\rho c u_2} \left(\frac{\bar{c}\bar{\kappa}\omega}{2}\right)^{\frac{1}{2}} \qquad (62).$$

To obtain the attenuation, α_s, due to thermal conduction at the side walls, consider a cylindrical resonator of cross-sectional area A, perimeter B, and symmetry axis in the z-direction. The amplitude of the temperature excursions, $\tilde{T}_o$, is proportional to $J_1 + J_2$, which, for strong reflection, is approximately $2J_1$. The amplitude decrease, $d\tilde{T}_o$, due to thermal conduction through an area Bdz at the side wall is proportional to $(J_1 - J_2)(Bdz/A)$. Thus, the effective attenuation is

$$\alpha_s \equiv -\frac{1}{\tilde{T}_o}\frac{d\tilde{T}_o}{dz} = \frac{J_1 - J_2}{2J_1}\left(\frac{B}{A}\right) \quad .$$

Using equation (61) gives

$$\alpha_s = (2/r\rho c u_2)\ (\bar{c}\bar{\kappa}\omega/2)^{\frac{1}{2}} \qquad (63)$$

for a cylinder of radius r.

C. Discussion of α_η, α_e, α_s

The inverse of the decay time is related to the total attenuation by $1/\tau = 2u_2\alpha$. From equation (52) the contribution to $1/\tau$ by viscous surface loss is

$$(1/\tau_\eta) = (2/r)(\rho_s/\rho)(\eta\omega/2\rho_n)^{\frac{1}{2}} \qquad (64).$$

This quantity has a strong dependence on ΔT, and becomes small for decreasing ΔT. In the analysis of results, $1/\tau_\eta$ is evaluated using the following expressions[42] ($t = \Delta T/T_\lambda$):

(i) $\rho_s/\rho = 2.534(t)^{.674}$

(ii) $\eta/\eta_\lambda = 1 - 5.19(t)^{.850}$ with $\eta_\lambda = 2.47 \times 10^{-5}$ poise

(iii) $\rho_n = \rho(1 - \rho_s/\rho)$ with $\rho = 0.146$ g cm^{-3} .

The contribution to $1/\tau$ from thermal conduction at the resonator ends is

$$1/\tau_e = (4/a\rho c)\ (\bar{c}\bar{\kappa}\omega/2)^{\frac{1}{2}} \tag{65}$$

where $\bar{c}$ and $\bar{\kappa}$ are those quantities for fused quartz glass. At the side walls thermal conduction contributes

$$1/\tau_s = (4/r\rho c)(\bar{c}\bar{\kappa}\omega/2)^{\frac{1}{2}} \tag{66}$$

with $\bar{c}$ and $\bar{\kappa}$ for stainless steel. The major temperature dependence in $1/\tau_e$ and $1/\tau_s$ comes from c, the specific heat of helium. The temperature dependence through $\bar{c}$ and $\bar{\kappa}$ is weaker in that they can be considered to vary primarily with T, not ΔT. An estimate using representative values[47] for $\bar{c}$ and $\bar{\kappa}$ indicates that $1/\tau_s$ is a factor of five greater than $1/\tau_e$. As the available information on $\bar{c}$, $\bar{\kappa}$ does not warrant an accurate evaluation of $1/\tau_e$ and $1/\tau_s$, and for reasons discussed in Chapter 4, in the final analysis of the data only the frequency dependence is used. Thus, the thermal conduction losses are treated collectively as $1/\tau_{\bar{\kappa}} = 1/\tau_e + 1/\tau_s$ with

$$1/\tau_{\bar{\kappa}} = g(T)\omega^{\frac{1}{2}} \tag{67}.$$

The function g(T) denotes the temperature dependence through c, $\bar{c}$, $\bar{\kappa}$.

Recall that an assumption involved in deriving (65) and (66) was $(2/\bar{c}\bar{\kappa}\omega)^{\frac{1}{2}} >> 1/G$. The validity of this approximation is difficult to assess due to the range of reported values for 1/G, reflecting its variability with material and detailed surface condition. Also measurements[48] of 1/G using an AC method involving coupled second sound resonators suggest that the value of 1/G for AC heat flow is much less than that measured with DC flows. If the AC data is taken as being representative of the present situation, then, at the highest frequency for the third harmonic of this experiment, the above inequality is satisfied by about

a factor of 100 for glass and eight for stainless steel. In view of the uncertainties involved, the validity of the approximation is subject to experimental verification.

The derivation of (67) involved use of (56), which is strictly correct only for a reflecting body of infinite extent. The approximation to a finite wall breaks down at sufficiently low frequencies when the thermal diffusion length, $(2\bar{\kappa}/\bar{c}\omega)^{\frac{1}{2}}$, becomes equal to the wall thickness. As it is estimated that this occurs at 40 Hz, a factor of three less than the lowest frequency obtained in this experiment, equation (67) is expected to apply.

CHAPTER 4

ANALYSIS OF DATA FOR THE DECAY RATE, $1/\tau$

The method used to determine the decay rate, $1/\tau$, from the chart recordings of the resonance decay curves is described in section A. Section B contains a discussion of several aspects of the results for $1/\tau$, including the frequency and temperature dependences. The results for D_2 are presented in section C.

A. Obtaining $1/\tau$ From Decay Curves

Figure 4 illustrates a decay curve representing the average of 150 individual decays of the third harmonic obtained at a temperature $\Delta T = 1.70(\pm 0.03) \times 10^{-4}$ K and frequency 588 Hz. In this example the second sound, generated by an input power density of 2×10^{-8} W cm^{-2}, had an initial amplitude of 5×10^{-8} K rms. Bias power in the bolometer was 1.2×10^{-6} W. The spike at the beginning of the trace results from the contribution of noise to the triggering threshold at which the decays are initiated. As can be seen, this noise remains coherent for a relatively short time and is ignored in an extrapolation to time zero when drawing the smooth curve through the trace. The amplitude of this smooth curve is normalized to unity and is used to determine the inverse decay time, $1/\tau$, from the slope of a plot of the natural logarithm of signal amplitude versus time. This plot is indicated in the inset of Figure 4.

It was mentioned in Chapter 2 that the decay rates are dependent on the power input to the cavity. Consequently, at each temperature several decay curves for the first and third harmonics were obtained for different values of the excitation power and bolometer bias power. Generally, for high values of the excitation power and bolometer power, the logarithmic

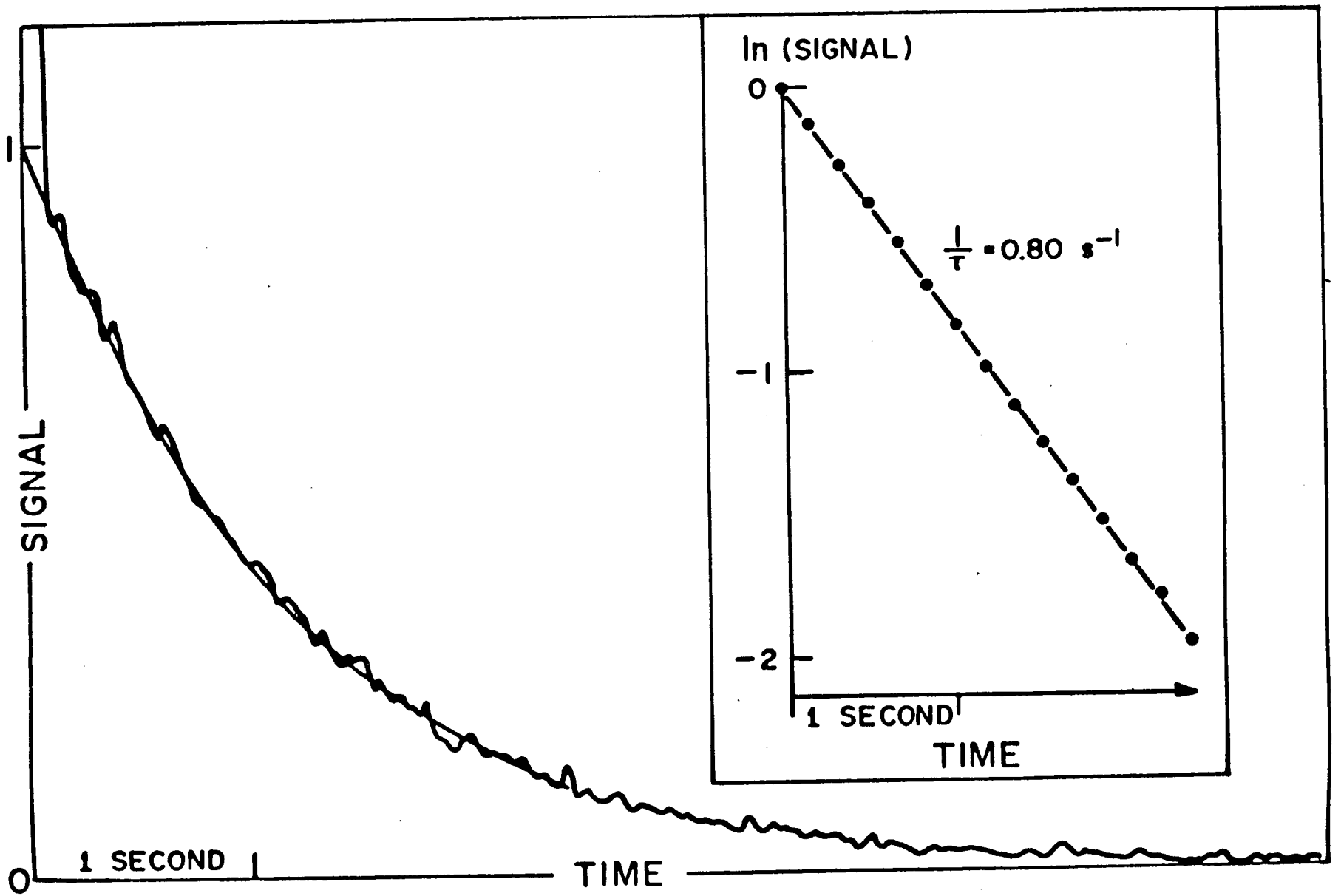

Figure 4 A Decay of a Second Sound Resonance Yielding a Value for the Decay Rate $1/\tau$

plots displayed a curvature indicating a larger value for the slope, $1/\tau$, at the beginning of the decay. At sufficiently low powers the curvature was not noticeable over the useful amplitude range (about 85% of full scale) of any particular decay. However, using even lower generator excitation powers indicated that there could still be a detectable amplitude dependence, a smaller value of $1/\tau$ occurring for those decay curves with a smaller initial second sound amplitude. A plot of the results for $1/\tau$ at $\Delta T = 1.70 \times 10^{-4}$ K for the third harmonic is given in Figure 5 to illustrate the nature of the extrapolations involved in determining the zero amplitude limit for $1/\tau$. At the highest bolometer and excitation powers, the presence of some curvature is the most significant contribution to the error estimates. For a given bolometer bias and lower excitation power the curvature diminishes or disappears and, as "goodness" of the fit to a simple exponential decay improves, the error estimates decrease. The errors are then limited primarily by the uncertainty in establishing the baseline of the decay curve in the presence of noise and small inaccuracies in the squaring circuitry. To obtain data at the lowest second sound amplitudes it was necessary to use the higher bolometer bias voltages in order to obtain an adequate signal. An extrapolation to zero amplitude, that is, zero excitation power, indicated by the line in Figure 5, is used to estimate a "best value" for $1/\tau$. As the extrapolation is subjective and without theoretical guidance, the associated error estimates, indicated by the shaded region in Figure 5, are treated generously according to the following criteria. The upper limit on the error estimate includes at least one value for $1/\tau$ that has been actually measured. Thus, the upper limit is determined with confidence. The lower limit on the error estimate is determined in a much more qualitative fashion by simply choosing a more severe extrapolation that is compatible

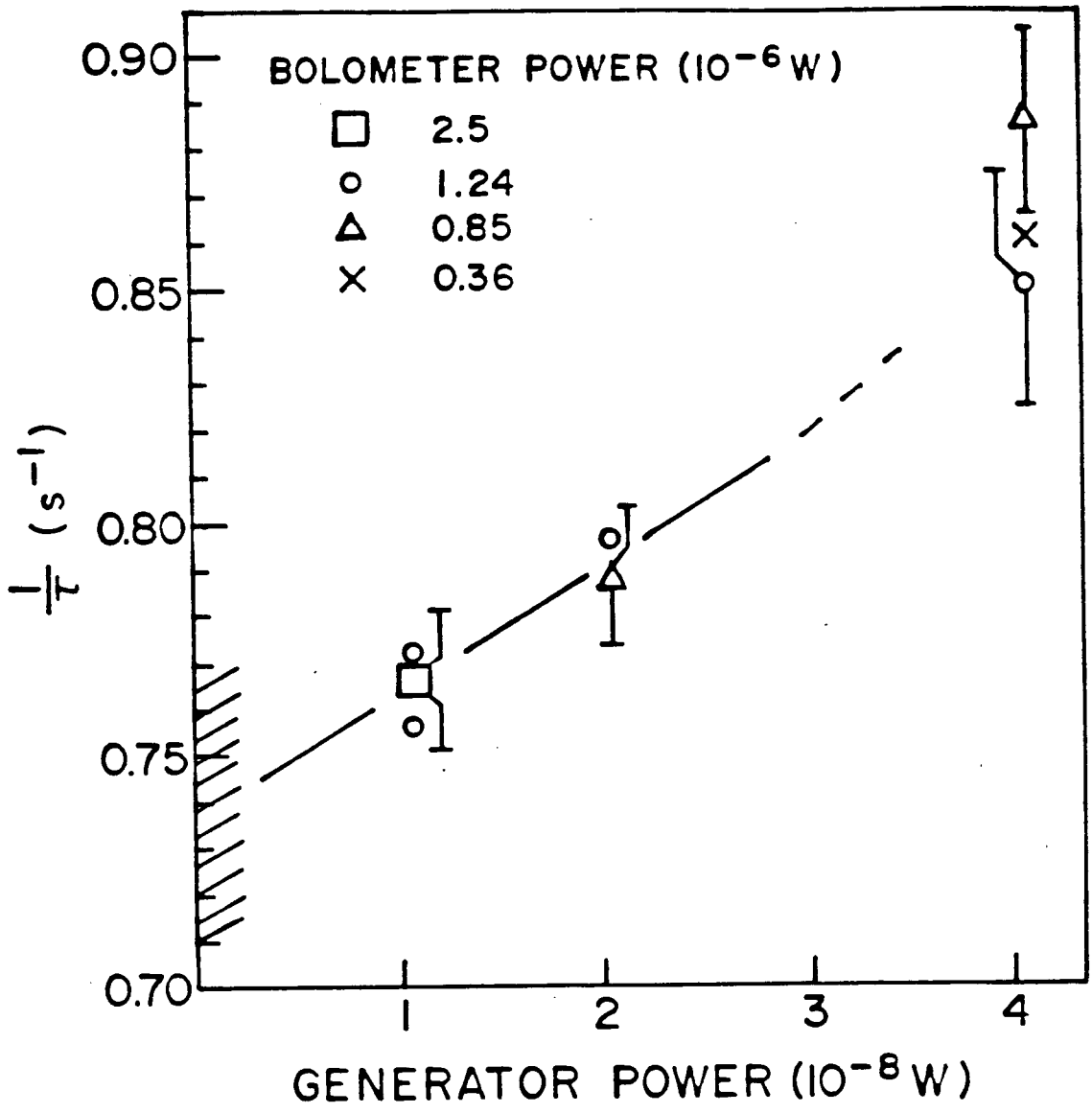

Figure 5 An extrapolation of values for $1/\tau$ to zero generator power for different levels of bolometer power. The extrapolation to zero amplitude, that is, zero excitation power in the generator, is used to estimate a best value for $1/\tau$. The hatched region indicates the error estimate. The data is for the third harmonic at $\Delta T = 1.70 \times 10^{-4}$ K.

with the measured values for $1/\tau$, or by symmetrically placing the lower limit a distance below the best value which is equal to the difference between the upper limit and best value. In the sense that this extrapolation procedure goes beyond the actual measurements of the experiment, the lower limits to the error estimate on $1/\tau$ are not determined with the confidence of the upper limits.

Generally, the amplitude effects for the first harmonic were not as significant as those for the third harmonic. Although at high amplitudes curvature similar to that for harmonic three was obtained, at lower amplitudes the extrapolated correction to zero amplitude was usually slight or insignificant for harmonic one. This observation suggests that the amplitude effects, at least at low amplitudes, result from additional loss mechanisms that are proportional to the bulk helium loss rather than surface losses. Recall the frequency dependence, ω^2 versus $\omega^{\frac{1}{2}}$, of the sources of attenuation described in Chapters 1 and 3. Then, comparing harmonic one to harmonic three, the contribution to $1/\tau$ from the bulk is fractionally smaller relative to the surface losses by a factor $9/\sqrt{3}$. Therefore, bulk related effects should be less significant at lower frequencies.

The effects of bolometer power were of two varieties. In one case the dependence of the decay rate on bolometer power was more significant at larger generator powers, or equivalently, larger second sound amplitudes. At the large amplitudes where curvature was present in the logarithmic plots of the decay, increasing the bolometer power resulted in a more severe curvature. However, at lower amplitudes where the curvature was smaller or not noticeable, the effects of changing the bolometer power were also smaller. At the smallest amplitudes a dependence on bolometer power was not resolvable within the accuracy of the measurements and ex-

trapolation to zero amplitude. Thus, corrections for bolometer power were usually not necessary. There was, however, a second type of dependence on bolometer power which was of an entirely different character compared to that described above. For the range of bolometer powers used in this experiment, there was an anomalous bolometer power at which enhanced losses occurred. The value of the anomalous power decreased through the range of available power levels as ΔT decreased through the temperature interval $4 \times 10^{-4} \leq \Delta T \leq 1 \times 10^{-3}$ K. The enhanced losses were not strongly dependent on second sound amplitude in that, at low amplitudes, the decay curves were governed by single time constants with the logarithmic plots showing no noticeable curvature. The magnitude of the enhanced losses at the anomalous power was about 50% of the zero power losses for harmonic one, and therefore the effect was quite dramatic. In addition, the value of the bolometer power at the anomaly was the same for the first and third harmonics and in this sense was independent of frequency. Also, the absolute magnitude of the enhanced losses appeared to be about the same for the first and third harmonics, although this was difficult to determine with precision since the normal amplitude effects confounded the observations. Since the enhanced loss was a sharp function at the anomalous bolometer power, it was possible, by operating either well above or below this power, to obtain meaningful data. It is emphasized that the enhanced losses diminshed with increasing bolometer power above the anomalous value, and for powers sufficiently removed from the anomaly the results became independent of bolometer power apart from the effects of the first variety described above. However, as stated above, in the interval $4 \times 10^{-4} \lesssim \Delta T \lesssim 1 \times 10^{-3}$ K the anomalous power was within the range of available bolometer powers and systematic effects, particularly for harmonic one, were observable. When operating within this interval at temperatures

$\Delta T = 1.02 \times 10^{-3}$ K and $\Delta T = 5.94 \times 10^{-4}$ K with the bolometer power less than the anomalous value, the best values for $1/\tau$ are obtained by extrapolation to zero bolometer power. For $\Delta T \leq 4.23 \times 10^{-4}$ K, the anomalous power is near or below the lowest useable bolometer powers. Then, the best values for $1/\tau$ correspond to the "high power" data; that is high power relative to the anomaly. Additional support for the general validity of the "high power" results is gained at $\Delta T = 3.05 \times 10^{-4}$ K. At this temperature the results of two additional decay curves for the second and fourth harmonics are consistent with the final results for D_2 based on the data for the first and third harmonics.

The mechanisms by which the bolometer power contributes to additional attenuation are not clear. The power dependent effects of the first variety described above can be qualitatively explained in relation to the second sound amplitude effects. If it is accepted that the amplitude effects simply reflect the departures from the zero amplitude requirements of linearized hydrodynamics, then the superposition of a DC counterflow, produced by the bolometer power, with the AC counterflow in the second sound would result in more severe violation of the requirement of small flow velocities. Of course, the situation in the cavity is further complicated by the asymmetry, AC versus DC flow, as well as the directionality of the flows, most of the DC heat leaving through the side walls while the AC flows are primarily parallel to the side walls. It is pointed out, however, that the DC flow velocities are at least a factor of two less than the rms flow velocities in the smallest amplitude second sound wave at the smallest value of ΔT in this experiment. The mechanism responsible for the additional losses of the second type described above is a mystery. If the curious reader wishes to speculate, he may consider the possible role played by vortices.

B. Discussion of the Data for $1/\tau$

As discussed in Chapters 1 and 3, the bulk helium damping, viscous surface losses, and thermally conducting surface losses contribute to $1/\tau$ as

$$1/\tau = 1/\tau_2 + 1/\tau_\eta + 1/\tau_\kappa \quad .$$

In terms of the damping coefficient D_2, the expression for $1/\tau_2$ is

$$1/\tau_2 = 2u_2\alpha_2 = (\omega^2/u_2^2)D_2 = (p\pi/a)^2 D_2 \qquad (68)$$

for harmonic "p" and resonant length "a". The expressions for the surface losses due to viscosity and thermal conduction, $1/\tau_\eta$ and $1/\tau_\kappa$ respectively, are given in equations (64, 65, 66, 67). The essence of the method involved in obtaining $1/\tau_2$ from the data for $1/\tau$ is to use the difference in frequency dependence, ω^2 versus $\omega^{1/2}$, between the bulk contribution and the surface contributions. To best illustrate this method and enhance the graphical presentation of the data, it is useful to compute $1/\tau_\eta$ according to the prescription in Chapter 3 and reduce $1/\tau$ to $1/\tau - 1/\tau_\eta$. This "correction" is significant for large ΔT. However, for $\Delta T < 1 \times 10^{-3}$ K, $1/\tau_\eta$ is numerically small and comparable to or less than the error estimates on $1/\tau$. In addition, it is useful to decompose the bulk contribution as follows:

$$1/\tau_2 = 1/\tau_{2HP} + \Delta(1/\tau_2) \qquad (69).$$

Here, $1/\tau_{2HP}$ denotes that value of $1/\tau_2$ which corresponds to the minimum value of D_2, 3.68×10^{-4} cm^2 s^{-1}, observed by Hanson and Pellam at a temperature $\Delta T = 3.2 \times 10^{-2}$ K. Thus, $1/\tau_{2HP}$ is just a constant which, using equation (68), is equal to 3.93×10^{-2} s^{-1} for harmonic one and 3.54×10^{-1} s^{-1} for harmonic three. The quantity $\Delta(1/\tau_2)$ represents changes from the minimum value observed by HP. Then the data for $1/\tau$ is further reduced to $1/\tau - 1/\tau_\eta - 1/\tau_{2HP}$ which is just $1/\tau_\kappa + \Delta(1/\tau_2)$. Although it

is necessary to correct the HP data to the "T_{58}" temperature scale[44], their values can be considered trustworthy in the sense that they have used a method of measurement that yields α_2 directly. As their results indicate only small changes in D_2 over the temperature range $1 \times 10^{-2} < \Delta T < 5 \times 10^{-2}$ K, $\Delta(1/\tau_2)$ is expected to be small over the interval. Thus, their results are used to "calibrate" the present system in the sense that they are used to check the validity of the predicted $\omega^{\frac{1}{2}}$ dependence for the surface losses, and to check the mode purity of the resonances (recall equation (38) for $\omega_{p,m,n}$ on page 27).

Before presenting the data for $1/\tau - 1/\tau_\eta - 1/\tau_{2HP} = 1/\tau_{\bar{K}} + \Delta(1/\tau_2)$, it is emphasized that the subtraction of $1/\tau_\eta$ from $1/\tau$ is done only as a convenience in the graphical presentation to remove a large, strongly temperature dependent contribution at large ΔT. As an indication of the magnitude and temperature dependence of $1/\tau_\eta$, some representative values of $1/\tau_\eta$, in units of s^{-1}, for the first and third harmonics are: 0.350, 0.607 at $\Delta T = 31.3 \times 10^{-3}$ K; 0.133, 0.231 at $\Delta T = 10.3 \times 10^{-3}$ K; 0.018, 0.031 at $\Delta T = 1.02 \times 10^{-3}$ K. Also, the subtraction of $1/\tau_{2HP}$ simply reduces the data by the appropriate constant value and provides a convenient way of displaying more clearly any changes, $\Delta(1/\tau_2)$, from the minimum value obtained by HP. In the final analysis, discussed in section C, the appropriate values of $1/\tau_{2HP}$ and $1/\tau_\eta$ are added to $1/\tau_{\bar{K}} + \Delta(1/\tau_2)$ to recover $1/\tau$.

The values of $1/\tau - 1/\tau_\eta - 1/\tau_{2HP}$ are shown in Figure 6 for harmonics one and three at temperatures such that $1.0 \times 10^{-3} < \Delta T < 4.6 \times 10^{-2}$ K. The solid lines are meant as visual aids. Several features of Figure 6 are discussed now.

Consider first the data for $p = 1, 3$. The solid smooth line drawn

Figure 6 The reduced decay rate $1/\tau - 1/\tau_\eta - 1/\tau_{2HP}$ for harmonics 1 and 3 as a function of ΔT for $1 \times 10^{-3} < \Delta T < 5 \times 10^{-2}$ K. $1/\tau_{2HP}$ is 3.93×10^{-2} s^{-1} for harmonic 1, and 0.354 s^{-1} for harmonic 3. The viscous surface loss, $1/\tau_\eta$, varies from 0.350 s^{-1} at ΔT = 31.3 mK to 0.018 s^{-1} at ΔT = 1.02 mK for harmonic 1, and is just $\sqrt{3}$ times greater for harmonic 3. The multiplicative factor, $\sqrt{3}$, indicated in the figure illustrates the $\omega^{\frac{1}{2}}$ frequency dependence of the surface losses, $1/\tau_\eta$, $1/\tau_{\_\kappa}$. Also indicated in the lower portion of the figure is the temperature dependence, relative to 1 mK, of the surface loss $1/\tau_{\_\kappa}$. The crosses represent the "observed" temperature dependence and are derived from the data for the first harmonic by removing the frequency dependence with the factor $[\omega_1(\Delta T)/\omega_1(1\text{ mK})]^{\frac{1}{2}}$. The solid circles represent the predicted behaviour as determined by the temperature dependence of the specific heat of helium.

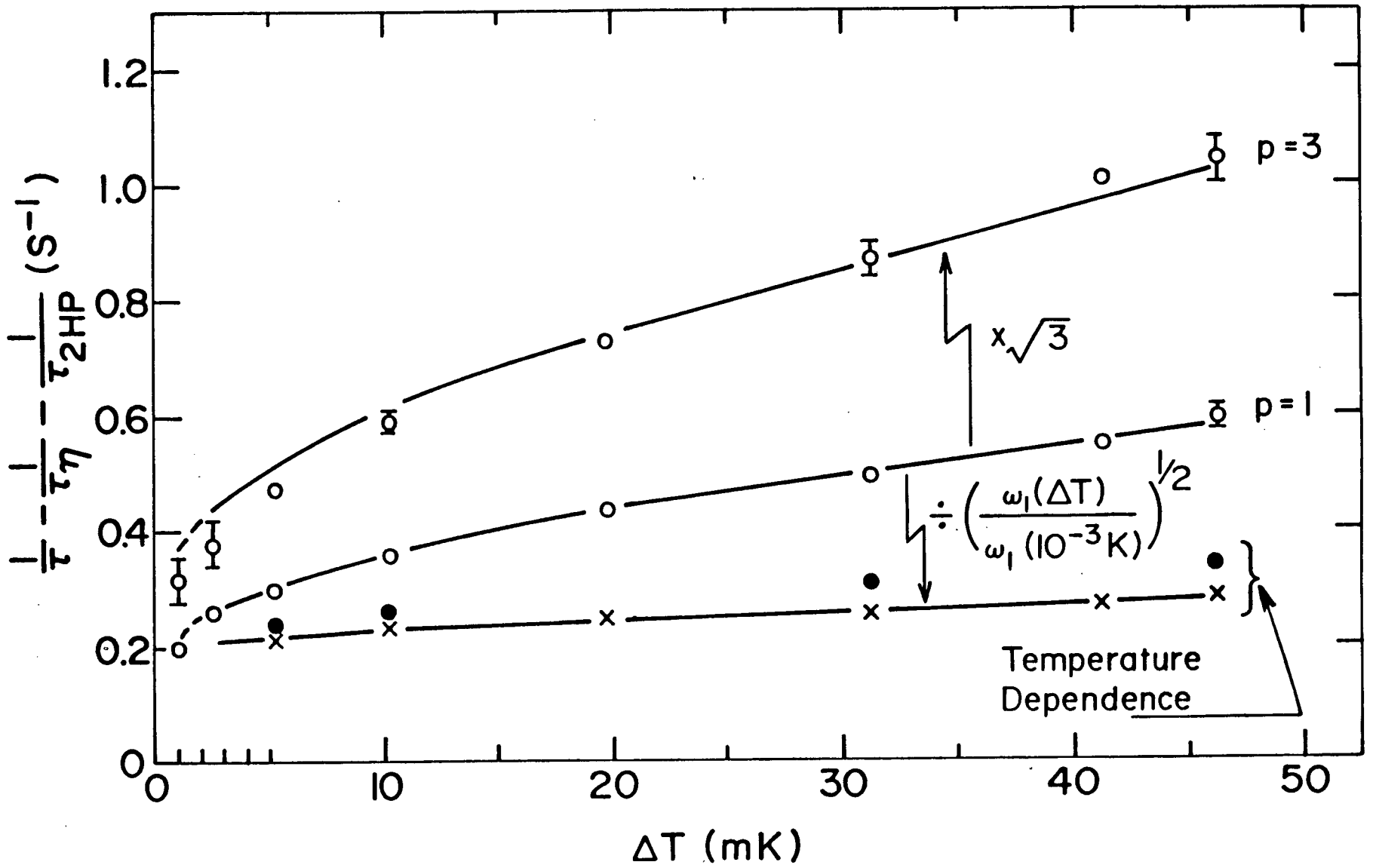
1.2
1.0
0.8
0.6
0.4
0.2
0
0
10
20
30
40
50
ΔT (mK)
$\frac{1}{\tau} - \frac{1}{\tau_\eta} - \frac{1}{\tau_{2HP}}$ (S^{-1})
p=3
p=1
x$\sqrt{3}$
$\div \left(\frac{\omega_1(\Delta T)}{\omega_1(10^{-3}K)}\right)^{1/2}$
Temperature
Dependence

through the data points for p = 1 yields, after multiplication by $\sqrt{3}$ as indicated, the solid line through the data points for p = 3. Since the major bulk attenuation contribution has been removed using the HP values, it is expected that $\Delta(1/\tau_2)$ is zero or very small in the temperature region around $\Delta T \sim 3 \times 10^{-2}$ K. Thus, on the basis of the good agreement between the p = 3 data and that derived form the p = 1 data using the multiplicative factor of $\sqrt{3}$, it is concluded that for the first and third harmonics, the contributions to $1/\tau$ from sources other than bulk damping are proportional to $\omega^{\frac{1}{2}}$.

The data for the third harmonic, at temperatures such that $1 \times 10^{-3} < \Delta T < 1 \times 10^{-2}$ K, falls below the line derived from the data for the first harmonic. Because the third harmonic is nine times more sensitive to changes in D_2 than the first, these deviations indicate a negative value for $\Delta(1/\tau_2)$, or equivalently, the bulk damping is falling below the minimum value observed by HP. Of course, the changes in D_2 are also present to a lesser extent in the data for the first harmonic and, therefore, the value of $1/\tau_2$ is determined by the solution, given in section C, to two simultaneous equations.

Finally, the temperature dependence of the surface losses is indicated by the crosses (x) in the lower portion of Figure 6. The smooth line through the crosses is a visual aid. This information is obtained as follows. The data for p = 1 contains both a temperature and frequency dependence. The latter is removed by dividing by the factor $[\omega_1(\Delta T)/\omega_1(10^{-3}\ \text{K})]^{\frac{1}{2}}$ where $\omega_1(\Delta T)$ is the frequency of the first harmonic at ΔT. In this way the surface losses are normalized to the measured value at 1×10^{-3} K, and any variations would reflect the temperature dependence. Of course, this requires that the frequency dependence, $\omega^{\frac{1}{2}}$, is

correct and that any significant corrections from $\Delta(1/\tau_2)$ in the data for $p = 1$ are accounted for. The expected temperature dependence, as predicted by equations (65) and (66), due to the specific heat of helium is indicated by the circles. Variations in the properties of the reflecting materials $(\bar{c},\bar{\kappa})$ have been neglected, and would only account for a small fraction of the difference between the observed and predicted frequency dependence. It is not clear what the source of the discrepancy is. It may indicate that the theory for $1/\tau_{\bar{\kappa}}$ is incomplete and that some consideration should be given to the details of the interface between the helium and the solid. For example, the presence of a viscous boundary layer might supress the losses due to thermal conduction. Alternatively, the theory for $1/\tau_\eta$ may be lacking. If the "true" viscous contributions to $1/\tau$ were 40% to 50% of the calculated values for $1/\tau_\eta$ that have been used in obtaining the data in Figure 6, then the observed differences would result. In any case, by measuring $1/\tau$ for both the first and third harmonics at each temperature, knowledge of the temperature dependence is not required to obtain D_2.

In a fashion similar to Figure 6, the results for $1/\tau - 1/\tau_{2HP} - 1/\tau_\eta$ for harmonics one, two and four are shown in Figure 7. The dashed lines, derived from the first harmonic by multiplication by $\sqrt{2}$ and 2, are expected to represent the contribution of $1/\tau_{\bar{\kappa}}$ to $1/\tau$. At $\Delta T \sim 3 \times 10^{-2}$ K it is evident, particularly for harmonic four, that there is some additional loss mechanism present which is not derivable from the first harmonic on the basis of an $\omega^{\frac{1}{2}}$ proportionality. It is noted, however, that the discrepancy of about 0.25 s^{-1} for harmonic four at $\Delta T \sim 3 \times 10^{-2}$ K is only about 10% of the total value for $1/\tau$. It is apparent that the discrepancy diminishes as ΔT decreases and, for $\Delta T \lesssim 3 \times 10^{-3}$ K, it is virtually insignificant. The results from three additional decay curves ob-

Figure 7 Similar to Figure 6, this figure shows the reduced decay rate $1/\tau - 1/\tau_{\eta} - 1/\tau_{2HP}$ for harmonics 1, 2, 4. The figure illustrates that there is an additional loss mechanism present for harmonics 2 and 4. The additional loss decreases with decreasing ΔT.

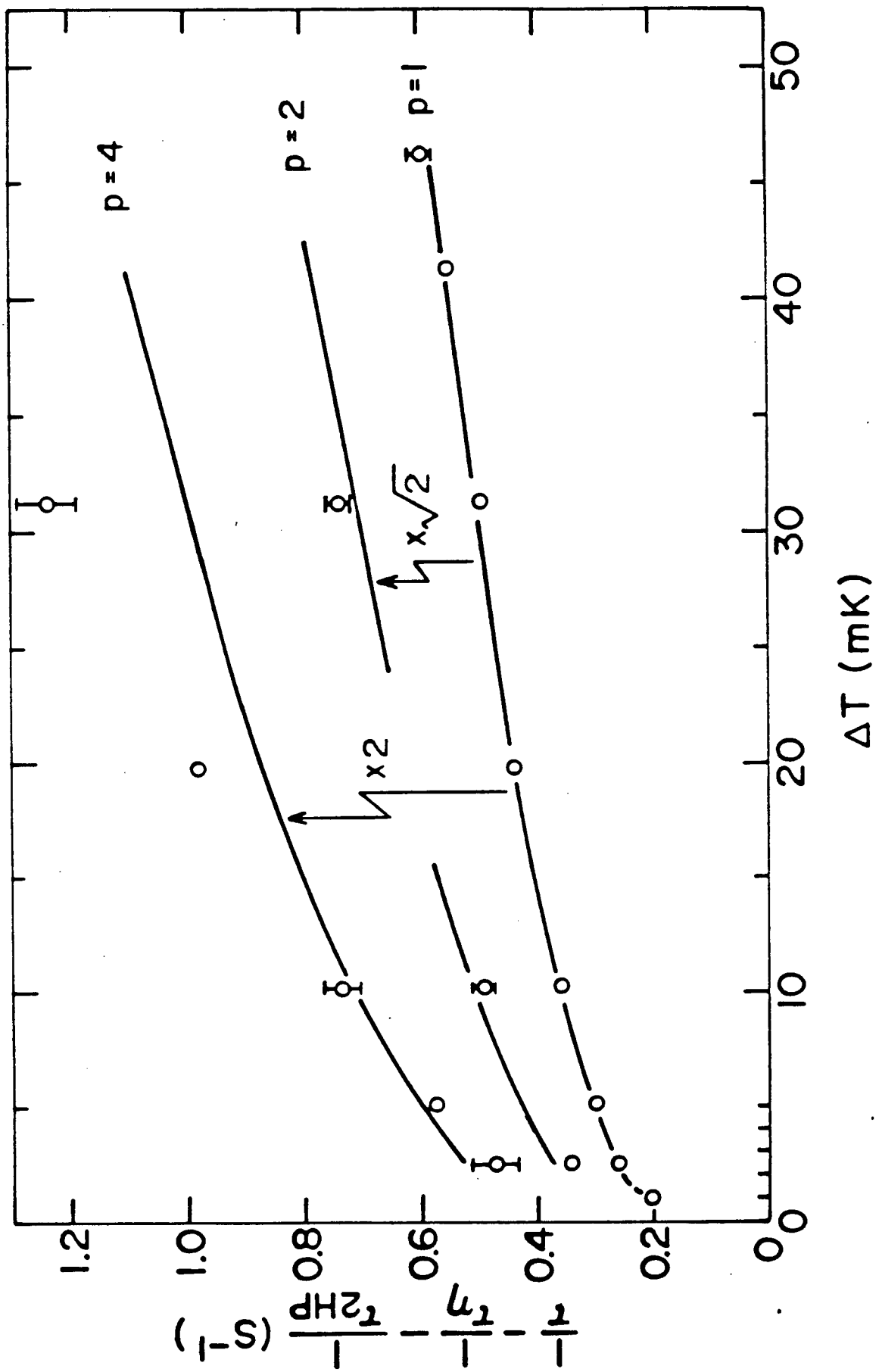
p=4
p=2
p=1
x2
x√2
1.2
1.0
0.8
0.6
0.4
0.2
0
10
20
30
40
50
ΔT (mK)
$\frac{1}{\tau} - \frac{1}{\tau_\eta} - \frac{1}{\tau_{2HP}}$ (S⁻¹)

tained for p = 2, 4 at $\Delta T = 3.05 \times 10^{-4}$ K and p = 2 at $\Delta T = 2.57 \times 10^{-3}$ K are consistent with the ultimate results for D_2 derived from the first and third harmonics.

The source of the additional loss appearing in the second and fourth harmonics at large ΔT is probably related to the associated resonant structure which appears when two harmonics, say two and four, are excited simultaneously as described in Chapter 2, section C. Mechanisms which could result in this additional loss by exciting Bessel modes are suggested in the general discussion of the final chapter. As a consequence of this discrepancy, only data for the first and third harmonics has been used in the final analysis for D_2.

The values of $1/\tau - 1/\tau_n - 1/\tau_{2HP} = 1/\tau_{\kappa} + \Delta(1/\tau_2)$ for the first and third harmonics over the entire temperature range covered in this experiment are shown in Figure 8. The critical damping is evidenced by the increase in the value of $\Delta(1/\tau_2)$ for the third harmonic as $\Delta T \to 0$. For $\Delta T < 10^{-2}$ K, the error estimates reflect the severity of the extapolations and the extent to which the data was collected at any particular temperature. For large ΔT the error estimates are due to the fractional resolution (1 or 2%) in determining $1/\tau$ with large surface contributions present. At the three smallest values of ΔT it is clear that the error estimates are increasing rapidly. This is a result of the severe extrapolations resulting from the amplitude effects described previously. As a matter of consistency with the data at larger values of ΔT, a best value and lower limit have been estimated at these three smallest values of ΔT; however, it is felt that the most significant information contained in these data points is the upper limit that these place on the ultimate values for D_2.

Figure 8 $1/\tau - 1/\tau_{\eta} - 1/\tau_{2HP}$ for harmonics 1 and 3 over the entire range of ΔT. Note that the temperature axis is logarithmic. The critical damping for $\Delta T < 10^{-3}$ results in the increasing separation of the data as $\Delta T \rightarrow 0$. The inset illustrates the frequency and temperature dependent contributions to the $p = 1$ data relative to 1 mK. The dashed line is derived by considering only the frequency dependence, while the solid line also includes the expected temperature dependence as determined by the specific heat, c, of helium.

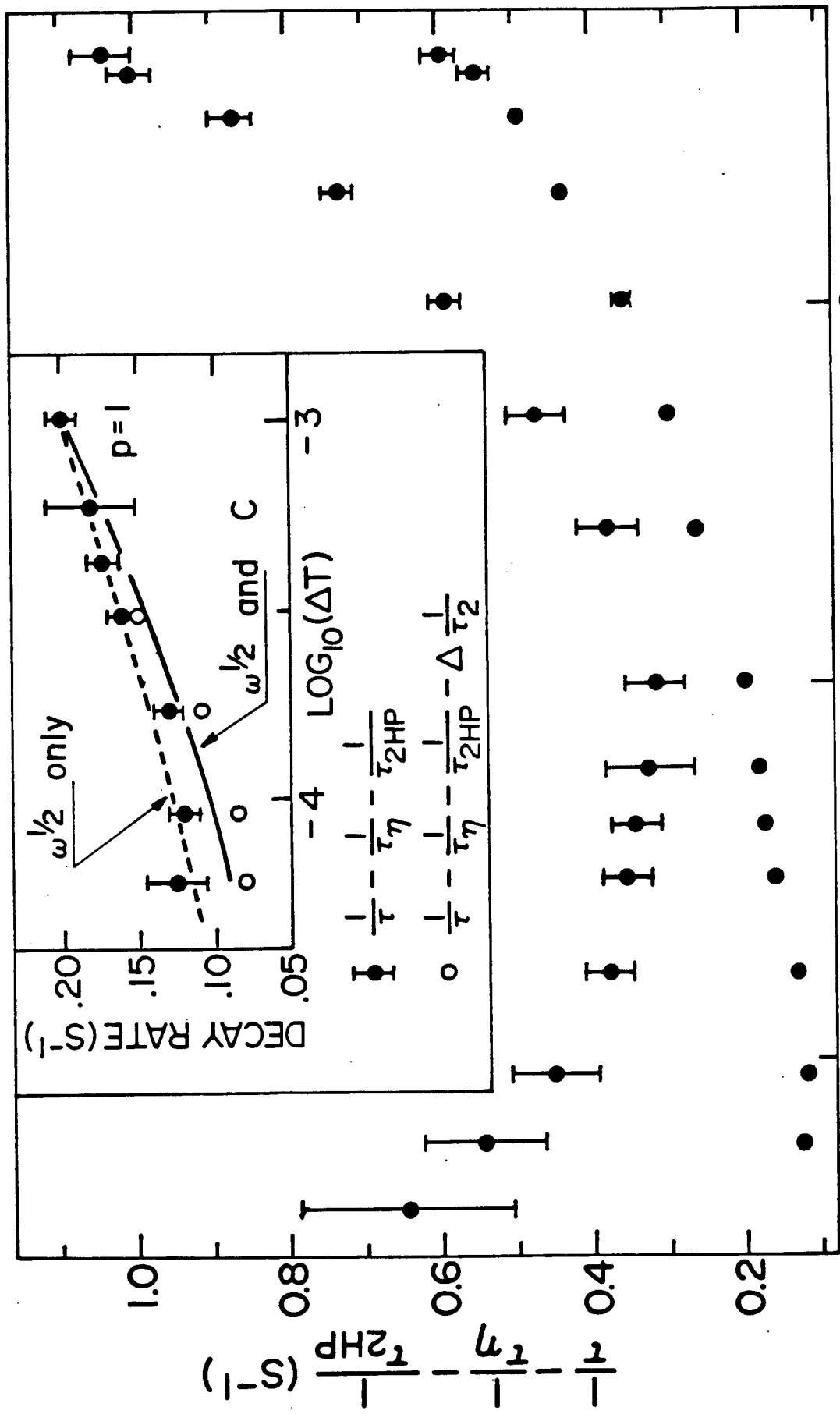
$\frac{1}{\tau} - \frac{1}{\tau_\eta} - \frac{1}{\tau_{2HP}}$ (S^{-1})
1.0
0.8
0.6
0.4
0.2
-4
-3
-2
LOG$_{10}$ (ΔT)
DECAY RATE (S^{-1})
.20
.15
.10
.05
-4
-3
LOG$_{10}$(ΔT)
$\frac{1}{\tau} - \frac{1}{\tau_\eta} - \frac{1}{\tau_{2HP}}$
$\frac{1}{\tau} - \frac{1}{\tau_\eta} - \frac{1}{\tau_{2HP}} - \Delta\frac{1}{\tau_2}$
ω½ only
ω½ and C
p=1

The inset of Figure 8 illustrates the predicted and observed behaviour of $1/\tau_{\bar{K}}$ for harmonic one and $\Delta T < 1.0 \times 10^{-3}$ K. The solid circles are the values for $1/\tau - 1/\tau_{\eta} - 1/\tau_{2HP} = 1/\tau_{\bar{K}} + \Delta(1/\tau_2)$. The open circles are derived from the solid circles by subtracting the contribution $\Delta(1/\tau_2)$ using the data for the third harmonic and the expression given in the following section. Thus, the open circles represent $1/\tau_{\bar{K}}$. The solid line represents the predicted behaviour of $1/\tau_{\bar{K}}$, relative to the value at $\Delta T = 1.0 \times 10^{-3}$ K, accounting for both the frequency dependence, that is, $\omega^{\frac{1}{2}}$, and the temperature dependence as determined by the specific heat, c, of helium. The dashed line results from considering only the frequency dependence. The temperature dependence of $1/\tau_{\bar{K}}$, as reflected by the departure from the dashed curve, is in qualitative agreement with the predicted solid line. Although it appears that there are systematic departures from the expected behaviour, the accuracy of the measurements is not sufficient to establish the precise form of these.

At $\Delta T = 4.0 \times 10^{-5}$ K it was difficult, because of noise, to obtain data for the first harmonic. Consequently, in the analysis for D_2, a value for $1/\tau_{\bar{K}}$ appropriate to the first harmonic is determined by a continuation of the open circles (or solid line) in the inset of Figure 8. In view of the relative uncertainty in $1/\tau$ for $p = 3$ at this temperature, and the small magnitude of the surface loss, this extrapolation does not introduce significant error.

C. Results for the Damping Coefficient, D_2

The inverse decay time for the first harmonic is described by an expression of the form

$$\frac{1}{\tau}^{(1)} = (D_2/u_2^2)\omega_1^2 + g\omega_1^{\frac{1}{2}} \quad .$$

Similarly, the expression for the third harmonic is

$$\frac{1}{\tau}^{(3)} = (D_2/u_2^2)\omega_3^2 + g\omega_3^{\frac{1}{2}} \quad .$$

With $\omega_3 = 3\omega_1$, these equations may be solved to obtain

$$\frac{1}{\tau_2}^{(3)} \equiv (D_2/u_2^2)\omega_3^2 = \left(\frac{1}{\tau}^{(3)} - \sqrt{3}\,\frac{1}{\tau}^{(1)} \right) [1 - (\sqrt{3}/9)]^{-1} \qquad (70)$$

which is the desired expression for $1/\tau_2^{(3)}$ in terms of the measured quantities $1/\tau^{(3)}$ and $1/\tau^{(1)}$. Using the dispersion relation $\omega = u_2 k$ and the resonance condition $k_p a = p\pi$, the expression relating D_2 and $1/\tau_2^{(3)}$ is

$$D_2 = (a^2/9\pi^2)\,\frac{1}{\tau_2}^{(3)} \qquad (71).$$

(To apply directly to the "reduced" data which has been presented in Figures 6 and 8, the appropriate expression for $1/\tau_2^{(3)}$ is

$$\frac{1}{\tau_2}^{(3)} - \frac{1}{\tau_{2HP}}^{(3)} = \Delta\frac{1}{\tau_2}^{(3)} = \{ \frac{1}{\tau_{\bar{K}}}^{(3)} + \Delta\frac{1}{\tau_2}^{(3)} - \sqrt{3} \left(\frac{1}{\tau_{\bar{K}}}^{(1)} + \Delta\frac{1}{\tau_2}^{(1)} \right)\}[1 - (\sqrt{3}/9)]^{-1} \ .)$$

The expressions (70), (71) are used to calculate D_2 from the measurements of $1/\tau^{(1)}$ and $1/\tau^{(3)}$. The numerical values for D_2 as a function of temperature are found in Table A in Appendix A. The results for $\log_{10} D_2$ are presented in Figure 9, including the theoretical predictions of HSH. The results are reproduced in Figure 10 which also includes the experimental results of HP[7], Tyson[10], Tanaka and Ikushima[12], Ahlers[13], and the theoretical predictions of HSH[14] and DF[15]. The results of this work are in good agreement with those of HP and Ahlers. In the critical region, which evidently extends to $\Delta T/T_\lambda = t \sim (0.5 \text{ or } 1) \times 10^{-3}$, there is confirmation of the renormalization group treatment of HSH. However, for $t \lesssim 10^{-3}$, the

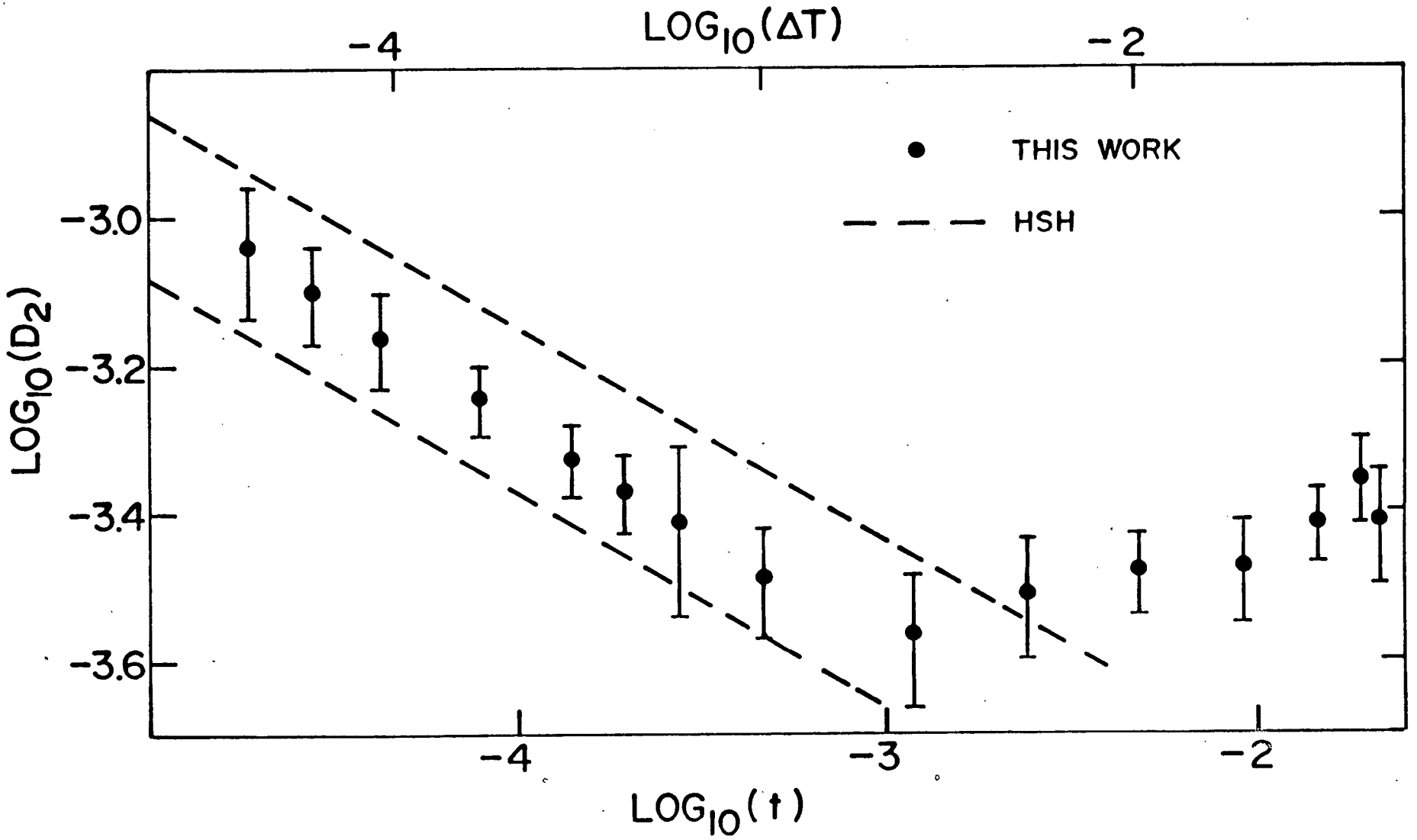

Figure 9 The Results for the Second Sound Damping Coefficient

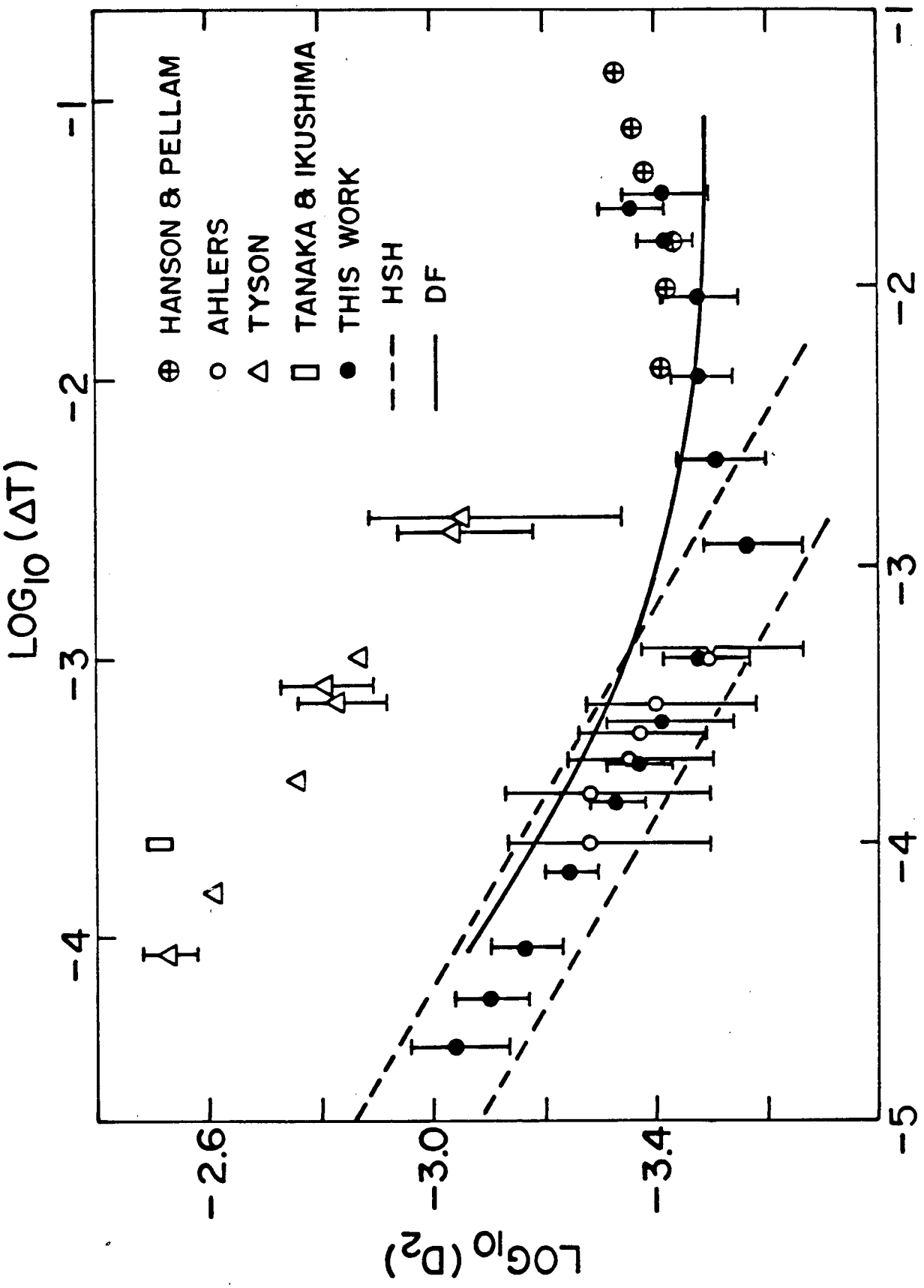

Figure 10

Summary of Results for the Second Sound Damping Coefficient

results are not in agreement with the theory of DF, and indicate values for D_2 which are less than their predictions. Considering the temperature dependence of D_2, the results are not sufficiently accurate to resolve any possible deviations from a single power law that might be interpreted in terms of a temperature dependent ratio, $R_2^{eff}(t) = D_2/2u_2\xi$, as predicted by DF.

A more quantitative comparison of this experiment and theory is achieved by describing the results in terms of the function $D_2 = D_{oex}t^{-\gamma_{ex}}$, with D_{oex} and γ_{ex} representing the experimental values for the amplitude and exponent for D_2. Considering the evident coherence of the data in Figure 9, it is tempting to use a least squares fit to the above function. However, it is felt that such a treatment, particularly with respect to the statistical estimate of a standard error, is unrealistic, and possibly misleading, in view of the possible (systematic) errors as represented by the error bars in Figure 9. A realistic , although subjective, estimate for γ_{ex} is

$$\gamma_{ex} = 0.31 \pm 0.05 \quad .$$

The subjective estimate of error, ± 0.05, is determined by evaluating, in Figure 9, the slopes of lines that are half way between the best fit and the extreme limits compatible with the error bars. Thus, while the results of this experiment do not provide a severe test of a detailed prediction for the critical temperature dependence, they do provide signifcant support for the appropriate type of critical behaviour for D_2 in the region $t < 10^{-3}$.

Since the amplitude, D_{oex}, is sensitive to the value of γ_{ex}, the best independent estimate for D_{oex} is obtained by constraining γ_{ex} to the theoretical prediction of $\gamma = 0.288$. Then the value of D_{oex}, again with

subjective consideration given to the possible systematic errors, is

$$D_{oex} = (3.7 \pm 0.4) \times 10^{-5} \text{ cm}^2 \text{ s}^{-1} \quad .$$

Of more general theoretical significance is the universal amplitude ratio, $R_2 = D_2/2u_2\xi$. This may be evaluated using the expressions for ξ and u_2 given at the end of Chapter 1 and the above value for D_{oex} obtained for $\gamma_{ex} = 0.288$, with the result

$$R_{2ex} = 0.11 \pm 0.01 \quad .$$

This experimental value lies between the theoretical values of HSH, 0.09 and 0.15, which are expected to be accurate to within a factor of two. The value for R_2^{eff} at $t = 10^{-4}$ as predicted by DF is about 0.14. However, as they do not indicate the accuracy of their calculation, it is difficult to assess the significance of the difference between R_{2ex} and R_2^{eff}.

CHAPTER 5

CONCLUSIONS AND DISCUSSION

Section A is a statement of the major conclusions of this work concerning the critical behaviour of the second sound damping coefficient, D_2. In section B there is a discussion of several general observations related to this experiment.

A. Conclusions

The damping of second sound in superfluid ^{4}He has been measured over the temperature interval $1.8 \times 10^{-5} < t < 2.1 \times 10^{-2}$. In the critical region the results, as illustrated in Figures 9 and 10, are in good agreement with the initial renormalization group treatment of D_2 by HSH[14]. However, the results do not support a recent renormalization group analysis by DF[15], the observed values for D_2 being less than the predicted values. The experimental result for the critical exponent, 0.31 ± 0.05, compares favourably with the predicted asymptotic temperature dependence, that is, $D_2 \sim u_2\xi$, with an exponent of 0.288. If the results are constrained to obey exactly the theoretical temperature dependence, then the experimental value for the amplitude D_{oex} defined by $D_2 = D_{oex}t^{0.288}$ is

$$D_{oex} = (3.7 \pm 0.4) \times 10^{-5} \text{ cm}^2 \text{ s}^{-1}.$$

The corresponding value for the universal amplitude ratio defined by $D_2/2u_2\xi$ is

$$R_{2ex} = 0.11 \pm 0.01 \quad .$$

In the common interval $10^{-4} < t < 5 \times 10^{-4}$, the results of this work are in good agreement with those of Ahlers[13]. For $t \gtrsim 10^{-3}$, it is observed that D_2 departs from its critical behaviour and increases to obtain the

values measured by HP[7].

B. Discussion

In this experiment the attenuation of second sound has been determined by measuring the decay time of plane wave modes in a resonant cavity. As opposed to measuring the resonant line-widths in a swept frequency method, the decay time technique possesses the significant advantage of being virtually immune to low frequency fluctuations in the ambient temperature. Consequently, this method may prove useful for future measurements of second sound damping at much smaller values of ΔT, as well as in studies of critical damping in other systems.

Tyson[10] used electrically thin resistive films to generate and detect second sound in his attenuation measurements. Ahlers[13], however, used porous superleak transducers. The discrepancy in their results suggested that there may have been some qualitative difference associated with the generation and detection devices. In view of the concurrence of the results of this work, which uses resistive devices, with that of Ahlers, it appears that there is not some fundamental disparity between the methods used to transduce second sound. There are, however, differences between the experimental methods of Tyson and this work which may account for the difference in results. Three major differences are described here. One involves Tyson's treatment of the reflection coefficient at the end walls of the resonator. In that experiment the reflection coefficient is assumed to be independent of frequency, and its contribution to the resonance widths is determined from an extrapolation of the total widths to zero frequency. In contrast, on the basis of this work there is theoretical and experimental evidence for a frequency dependent reflection coefficient, although at sufficiently high frequencies the presence of a Kapitza res-

istance could result in the reflection coefficient becoming frequency independent. A second difference is that the input power densities used by Tyson are at least an order of magnitude greater than the power levels used in this experiment. Although Tyson extrapolates to zero power, this procedure might introduce systematic errors that could account for the difference in results. The third difference is that in Tyson's experiment the absence of side walls in the resonator required a correction to the resonance widths involving diffraction loss. In the resonator of this experiment there are side walls present which eliminate diffraction loss, but introduce viscous and thermal conduction losses. Although the calculated diffraction loss in Tyson's experiment is small or insignificant, early studies in this work on a cavity without side walls gave results that were difficult to interpret on the basis of diffraction from a plane-wave resonance. Indeed, the frequencies of the major resonances did not correspond to a harmonic series $\omega_{p,0,0}$ for p = 0, 1, ... 5, but rather to a series with a Bessel mode character corresponding to $\omega_{p,0,1}$ or $\omega_{p,1,0}$. At higher frequencies such that p > 10, the resonances did not display a single mode character, but contained several peaks resulting from overlapping modes. Subsequent studies with a variety of boundary conditions at the sides indicated that the resonant structure was sensitive to the details of the side boundary. As a result, the simplest, "ideal", side wall described in Chapter 2 was finally used.

Although care was taken to prevent the excitation of Bessel modes in the cavity, they were, nevertheless, excited. A general mechanism responsible for their excitation is suggested on the basis of the following observation made in this experiment. It was found that Bessel modes in the vicinity of a plane wave harmonic were excited, while deep in the region between the plane wave harmonincs there were no Bessel modes visible. This

indicates that the excitation proceeds by way of the plane wave resonance. Once the relatively large energy excursions in a resonance are established, a small perturbation at the walls of the cavity is capable of directing a significant portion of the energy into the excitation of another mode. As an example, the viscous loss occurring at the side walls of the cylindrical cavity could result in a temperature and velocity profile in the radial direction which is not flat, but instead, curved at the edges near the wall. This profile could then establish an energy flow in the radial direction and excite a Bessel mode. This type of mechanism could account for the excess loss in harmonic four, where it is observed that the excess loss diminishes as the frequency and ΔT, and therefore the viscous loss, decrease. Other factors that could excite Bessel modes by developing angular and radial variations in the cavity include thermal conduction losses through the side walls, and the possibility of a variable reflection coefficient, due to power dissipation, across the face of the bolometer.

Progress has been made in understanding the loss mechanisms occurring at the walls of a resonant cavity, although there is some difficulty in interpreting the observed temperature dependence. Systematic studies on several resonant cavities of different dimensions and materials would likely solve this problem and, in addition, provide some information about the contribution of the Kapitza resistance to the reflection of second sound. While it is doubtful that the knowledge gained from such studies is in itself worth the effort, the information would be useful in optimizing the cavity geometry for further improvements in the measurement of the critical damping of second sound. Thus, for example, by using a longer cavity for a given radius, one should obtain more clean plane wave modes that are useable for attenuation studies. However, if the overall resolution of the experiment is to improve, the frequency of the highest

useable mode must not decrease due to the interference of nearby Bessel modes. To ensure that the frequency range is maintained it might be possible to design the cavity to critical tolerances in the radius-to-length ratio, r/a, in order to avoid Bessel modes.

While consideration must be given to the possible means of improvement available through changes in the resonator geometry and materials, it is also important to overcome the effects on attenuation due to second sound amplitude and bolometer power. Although small amplitudes and low power have been used in this experiment, these, nevertheless, have limited the ultimate accuracy at the smaller values of ΔT. To recover lower level signals, enhancement of the signal to noise ratio could be made with improvements to the bolometer. Experience with several bolometer films suggests that the sensitivity can be increased by at least a factor of two. Also, increasing the bolometer resistance with a more intricate pattern design would increase the signal level and provide a better impedance match to the noise figure of the existing electronics, although some care must be taken with this procedure as it ultimately reduces the active area of the bolometer. Another immediate improvement which, unfortunately, was not taken advantage of, involves using different electronics in order to obtain a lower noise figure at the initial stages of amplification. For example, with the bolometer resistance and frequencies of this experiment, an appropriate input transformer and preamplifier[49] would reduce the amplifier noise by about a factor of two. Although noticeable, the extent to which this factor would be realized in the overall signal to noise ratio depends on the strength of other noise sources such as pickup in the leads and "intrinsic" bolometer noise. In terms of future work, a more useful and flexible low noise input that also reduces

the effect of lead pickup would be a low temperature preamplifier.

Then, achieving a final accuracy in D_2 on the level of a few percent, it would be possible to provide detailed information of the temperature dependence of D_2. It would also be worthwhile to perform the measurements at elevated pressures as a test of universality.

REFERENCES

1. H.E. Stanley, Introduction to Phase Transitions and Critical Phenomena (Oxford University Press, New York, 1971).

2. L.D. Landau and I.M. Khalatnikov, Dokl. Akad. Nauk SSSR 96, 469 (1954); reprinted in Collected Papers of L.D. Landau, edited by D. ter Haar (Gordon and Breach Science Publishers Ltd. and Pergamon Press Ltd., New York, 1965).

3. L.P. Kadanoff, W. Götze, D. Hamblen, R. Hecht, E.A.S. Lewis, V.V. Paliciauskas, M. Rayl, J. Swifts, D. Aspnes, and J. Kane, Rev. Mod. Phys. 39, 395 (1967).

4. B.I. Halperin and P.C. Hohenberg, Phys. Rev. 177, 952 (1969); R.A. Ferrell, N. Menyhard, H. Schmidt, F. Schwabl, and P. Szépfalusy, Ann. Phys. 47, 565 (1968).

5. K.G. Wilson and J. Kogut, Phys. Rep. 12C, 76 (1974); K.G. Wilson, Rev. Mod. Phys. 47, 773 (1975); M.E. Fisher, Rev. Mod. Phys. 46, 597 (1974).

6. P.C. Hohenberg and B.I. Halperin, Rev. Mod. Phys. 49, 435 (1977).

7. W.B. Hanson and J.R. Pellam, Phys. Rev. 95, 321 (1954).

8. J.A. Tyson, Phys. Rev. 166, 166 (1968).

9. D.S. Greywall and G. Ahlers, Phys. Rev. A 7, 2145 (1973).

10. J.A. Tyson, Phys. Rev. Lett. 21, 1235 (1968).

11. Light scattering measurements probe "microscopic" second sound. See reference 6 and references therein.

12. M. Tanaka and A. Ikushima, J. Low Temp. Phys. 35, 9 (1979).

13. G. Ahlers, Phys. Rev. Lett. 43, 1417 (1979).

14. P.C. Hohenberg, E.D. Siggia, B.I. Halperin, Phys. Rev. B 14, 2865 (1976); E.D. Siggia, Phys. Rev. B 13, 3218 (1976).

15. V. Dohm and R. Folk, Phys. Rev. Lett. 46, 349 (1981).

16. I.M. Khalatnikov, An Introduction to the Theory of Superfluidity (W.A. Benjamin Inc., New York, 1965). The initial paper by Landau on the quasi-particle theory is reprinted at the back of this book.

17. P.C. Hohenberg and P.C. Martin, Ann. Phys. 34, 291 (1965).

18. S. Putterman, Superfluid Hydrodynamics (North Holland Publishing Company, Amsterdam, 1974).

19. At $\Delta T = 2 \times 10^{-5}$ k, $(c_p - c_v)/c_p = 3.6 \times 10^{-2}$; see reference 42 for a discussion of the significance of $(c_p - c_v)/c_p$.

20. L.P. Kadanoff and P.C. Martin, Ann. Phys. 24, 419 (1963).

21. P.W. Anderson, Rev. Mod. Phys. 38, 298 (1966).

22. B.I. Halperin, P.C. Hohenberg and E.D. Siggia, Phys. Rev. B 13, 1299 (1976).

23. T. Matsubara and H. Matsuda, Prog. Theor. Phys. 16, 569 (1956).

24. B.I. Halperin and P.C. Hohenberg, Phys. Rev. 188, 898 (1969).

25. T. Worthington, J. Yan and J.U. Trefory, J. Low Temp. Phys. 24, 365 (1976).

26. P.M. Morse, Vibration and Sound (McGraw-Hill Book Company Inc., New York, 1948). Also, P.M. Morse and H. Feshbach, Methods of Theoretical Physics (McGraw Hill Book Company Inc., New York, 1953). A large table for the α_{mn} is in M. Abromonitz and I.A. Stegun (eds.), Handbook of Mathematical Functions, page 411, (Dover Publications Inc., New York, 1965).

27. E.J. Walker, Rev. Sci. Inst. 30, 834 (1959).

28. D. d'Humieres, A. Launay, and A. Libchaber, J. Low Temp. Phys. 38, 207 (1980).

29. H.S. Carlsaw and J.C. Jaeger, Conduction of Heat in Solids, (Oxford University Press, 1959).

30. H.L. Caswell, Phys. Lett. 10, 44 (1964).

31. Measured with a Digital Thickness Monitor DTM - 200 manufactured by Sloan Technology Corporation, Santa Barbara, California.

32. John Fluke Mfg. Co., Inc., Seattle, Washington; model 6010 A.

33. Princeton Applied Research Corporation (P.A.R.C.), Princeton, New Jersey; model 5204.

34. P.A.R.C. model 114 with 118 option.

35. Teledyne Philbrick multiplier/divider model 4452.

36. Nicolet Instrument Corporation, Madison, Wisconsin; model 1170.

37. Electro Scientific Industries, Portland, Oregon; model DT 72 A.

38. P.A.R.C. model 114 with 185 option.

39. P.A.R.C. model 112.

40. The feedback circuitry was of personal design and made with standard solid state operational amplifiers.

41. General purpose tunnel diode 1N3714. A description of this type of circuit can be found in C. Boghosian, H. Meyer, and J.E. Rives, Phys. Rev. 146, 110 (1966).

42. G. Ahlers in The Physics of Liquid and Solid Helium, edited by J.B. Ketterson and K.H. Benneman (John Wiley and Sons, New York, 1976), Vol. I.

43. B. Robinson, MSc Thesis, U.B.C. (1976); see also reference 8.

44. The thermometer was calibrated by vapour pressure thermometry against "1958 He^4 Scale of Temperatures", United States Department of Commerce, National Bureau of Standards, Monograph 10 (1960).

45. J. Heiserman and I. Rudnick, J. Low Temp. Phys. 22, 481 (1976).

46. I.M. Khalatnikov, Usp. Fiz. Nauk. 60, 69 (1956). (English translation available in Univ. of California Radiation Lab. Transl. 675; also, Hydrodynamics of Helium II with U.B.C. library listing QD 181 H4 K5 1956).

47. G.K. White, Experimental Techniques in Low-Temperature Physics (Oxford University Press, London, 1968); WADD Technical Report 60-56 Part II (1960), A Compendium of Properties of Materials at Low Temperatures (Phase I), by V.J. Johnson of the National Bureau of Standards, Cryogenic Engineering Laboratory.

48. N.J. Brow and D.V. Osborne, Phil. Mag. 3, 1463 (1958).

49. P.A.R.C. model AM1 with, for example, P.A.R.C. model 114 with 119 option.

APPENDIX A

TABLE A

Results for D_2

ΔT(K)	$t = \Delta T/T_\lambda$	D_2 (10^{-4} cm^2 s^{-1})
4.62×10^{-2}	2.13×10^{-2}	3.86 ± 0.7
4.12×10^{-2}	1.90×10^{-2}	4.39 ± 0.6
3.13×10^{-2}	1.44×10^{-2}	3.83 ± 0.5
1.97×10^{-2}	9.07×10^{-3}	3.35 ± 0.5
1.03×10^{-2}	4.74×10^{-3}	3.31 ± 0.4
5.17×10^{-3}	2.38×10^{-3}	3.09 ± 0.6
2.57×10^{-3}	1.18×10^{-3}	2.72 ± 0.6
1.02×10^{-3}	4.70×10^{-4}	3.26 ± 0.6
5.94×10^{-4}	2.74×10^{-4}	3.88 ± 1.0
4.23×10^{-4}	1.95×10^{-4}	4.24 ± 0.5
3.05×10^{-4}	1.40×10^{-4}	4.70 ± 0.5
1.70×10^{-4}	7.83×10^{-5}	5.69 ± 0.6
9.10×10^{-5}	4.19×10^{-5}	6.86 ± 1.0
5.95×10^{-5}	2.74×10^{-5}	7.92 ± 1.2
4.00×10^{-5}	1.84×10^{-5}	9.14 ± 1.8